UNIVERSITY OF TWENTE.

**Faculty of Electrical Engineering,**
**Mathematics & Computer Science**

# MFManufacturing: porting the fertility chip to the standard platform

**T. Feijten**

**Master thesis**
**August 2017**

Exam committee:
Stefan Dekker, MSc
Dr. Mathieu Odijk
Prof. dr. ir. Albert van den Berg
Dr. Susan Roelofs
Prof. dr. ir. Gijs Krijnen

Report number: 2017-4
Faculty of Electrical Engineering,
Mathematics and Computer Science
University of Twente
P.O. Box 217
7500 AE Enschede
The Netherlands

# MFManufacturing: porting the fertility chip to the standard platform

T. Feijten, S. Dekker, A. van den Berg, M. Odijk

Male fertility testing is a cumbersome procedure, involving multiple visits to the hospital to deliver a sperm sample. The testing itself is a laborious and error-prone process. Point of care (PoC) testing can play a crucial role in making this a more comfortable and reliable experience. In the past, a system has been developed based on impedance spectroscopy to perform the diagnosis. However, it is not yet ready for PoC applications or home testing, because the current set-up is bulky. This work tackles some of the problems involved, in porting it to a standard platform and increasing the measurement accuracy by implementing a differential measurement method. Impedance deviations down to 0.22‰ are detected with headroom available. This shows the potential of this solution for fertility testing.

## 1 Introduction

Cellanyzer BV is in the progress of developing a point-of-care (PoC) device for fertility testing based on the proof-of-concept as shown by Segerink et al[1]. However, to get the product to market a few difficulties are encountered: the results are not reliable enough to draw definitive conclusions[2,3], the peripheral devices (impedance spectroscope, transimpedance amplifier, syringe pump, PC) are quite bulky, the used capillaries are prone to leakage and the electronics are prone to noise. These kind of difficulties are encountered in the commercialization of many more microfluidic devices[4]. To get towards a device that can be used in a PoC setting, these difficulties will have to be dealt with.

### 1.1 Fertility testing

For many couples wanting to start a family (1 out of 6[5]), fertility is an important issue. In most cases, the first diagnostic test to be run concerns the sperm of the man, as this is easily testable and a main inhibiting factor in 30% of the cases[5]. In this test, the amount and motility of the sperm is investigated. The reference values for this, as given by the World Health Organisation (WHO) in 2010, are $15 \cdot 10^6$ spermatozoa per mL or more, of which 40% or more should be motile[5].

The current golden standard for diagnosing these parameters is by getting a sperm sample from the man, which is then partly injected in a haemocytometer (microscope slide with measurement grid and known volume per unit area) and stained. The cells are then counted and classified as being motile or non-motile[5]. As this is a time-consuming (therefore costly) process in which the probability of human error or difference in opinion is large, it is not an optimal process.

To solve some of the problems stated in the previous paragraph, an objective method has been developed. This method is based on the established concept of microfluidic Coulter counters, which are devices that measure the impedance change due to an object moving along two electrodes. For an equivalent circuit diagram without a cell, see Figure 2. When a cell passes the area between the electrodes, the resistance of $R_{el}$ changes, which can be detected[1]. To validate the performance of such devices, often microbeads made from polystyrene are used. These devices have been shown (amongst others) to work for assessing yeast cell growth[6], assessing airborne mineral dust[7] and cell counting[1,8], which can also be integrated on CMOS-platforms[9].

To measure the impedance, a couple of methods can be utilized. Simply said, one needs a potential difference and a current ($Z(t) = \frac{U(t)}{I(t)}$) to determine the impedance. Potentials are commonly used to actuate, therefore, in a simple set-up, only the current needs to be determined (2-wire measurement). In a 4-wire measurement, the potential difference is determined as well to increase the accuracy. In this work, a 2-wire measurement will be used. To determine the current, one can use a resistor to convert it to a potential difference, which is easy to convert to a signal using, for instance, an Analog to Digital Converter (ADC). However, this resistor will influence the potential difference of the electrode pair on the fertility chip, leading to problems when non-linear effects are in place. To circumvent these problems a Transimpedance Amplifier (TIA, see Figure 1) can be used, which uses an op amp to convert the current to a potential difference. Because of the high input impedance of the op amp, the current will flow through the feedback resistor, causing an output potential which can be measured. Resistors are prone to thermal noise, which can be a problem for very noise-sensitive applications. As capacitors don't have this issue, alternative implementations have been suggested to be used as a TIA, using capacitors as feedback system[10–13].

To further improve the performance (the measured difference can be very small), an impedance spectroscope containing a lock-

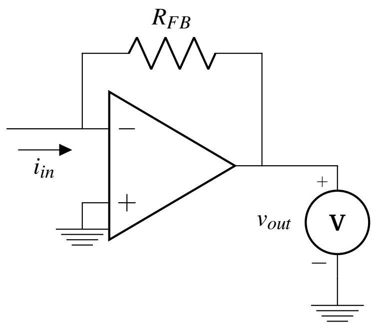


**Fig. 1** Traditional transimpedance amplifier circuit to convert a current to a potential difference. Due to the high input impedance of the op amp, the current will flow through the feedback resistor, leading to a potential difference at the output terminal.

in amplifier can be utilized. Using mixing and filtering, out-of-band noise is decreased drastically, which increases the signal-to-noise ratio (SNR) [14].

In the system, the information is contained in the change of impedance, which can be as small as 0.1‰. The background impedance of the electrolyte and other parts of the system, therefore, is not important, but it takes up a major part of the dynamic range of the measurement device. To optimize the measurement for the dynamic range of the lock-in amplifier and reduce noise, it is worthwhile to set up a differential measurement [15].

### 1.2 Standardization

For microfluidics, no easy prototyping process exists. The main reason for this is that standard components, performing a specific function (for instance mixing, separating or sensing), are not available. This also means that interconnects are not standardized, leading to difficulties when integrating components provided by external parties. This is detrimental for the fabrication of prototypes, making it very hard to go from an idea to production-ready prototype.

To solve these problems, a system analogous to electronics could be used. In electronics, the usual design strategy is to design a circuit using commercial off-the-shelf integrated circuits (ICs) and discrete components, such as capacitors, resistors and diodes. This design can then be implemented by producing a printed circuit board (PCB), on which the ICs and discrete components are soldered. This makes for a very flexible and quick prototyping process, which drives the industry.

Multiple solutions for this problem have been proposed [16], including a modular hybrid platform using flexible PCBs, which improves the integration of electronics and microfluidics [17], spinning plastic disks, which are a step ahead of prototyping, focussing on mass production [18], reconfigurable digital chips for PoC testing, which are mainly suited for fluidic mixing and sample preparation [19] and paper-based devices, which are interesting for resource-limited settings, quantitative readouts can be achieved via external devices [20].

This work will use the prototyping platform designed by the MFManufacturing consortium [21,22]. It consists of an inherent split between functional blocks (Microfluidic Building Blocks, or MFBBs) and interconnects (Fluidic Circuit Board, or FCB). The interface of the MFBBs follows a standard, making it fairly easy to design and fabricate an FCB on which the desired MFBBs can be placed. The MFBBs can then be bought from an external party, analogous to ICs, and the FCB doesn't contain any functionality except for interconnections, making it easy to design. This modular platform is very well suited for development in a lab setting. To accelerate the maturation of this platform, projects like this work can use it to test the platform and improve the applicability.

### 1.3 This work

To get the fertility device ready as a prototype, this work will propose and implement some improvements. To improve the reliability of the results and the sensitivity of the electronics, a new differential circuit will be designed, produced and tested. To remove the capillaries and reduce the size of the peripherals, the device will be implemented based on the MFManufacturing platform.

First an explanation of the design choices and some simulations will be given, after that the practical considerations will be treated. Then, the results will be discussed. Finally, a conclusion will be drawn and some recommendations for future research will be given.

## 2 Design & Simulation

### 2.1 Design requirements

Considering the information given in the introduction and general considerations for a PoC device [23], a set of requirements can be composed for the system:

1. The system should incorporate the 15x20mm fertility chip as made by Segerink et al [1];
2. The system should be compliant with the standard as set forth by MFManufacturing [21,22];
3. The system should reliably determine the concentration of a sperm sample within a margin of $10^4$ cells per mL;
4. The measurement result is available at most 5 minutes after introduction of the sample;
5. Between loading the sample and reading out the measurement, no user interaction should be needed;
6. The system can function at temperatures between 10 °C and 40 °C;

Using these requirements, a system has been designed. It consists of an FCB which can accommodate the fertility chip, and assisting electronics for the first signal processing, after which the signal will be processed using the lock-in amplifier.

### 2.2 Impedance detection

The impedance of a microfluidic channel, for which the equivalent circuit diagram is given in Figure 2 and which can be measured by two electrodes, depends on the contents of the channel. In Figure 3a, an impression is given of the field lines for

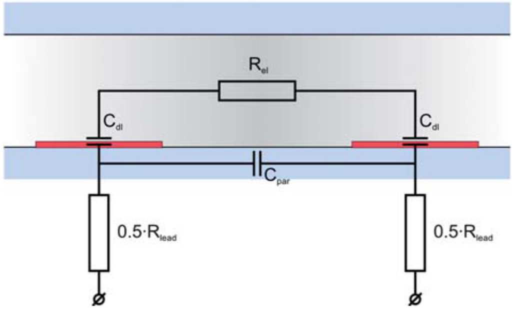


**Fig. 2** Equivalent circuit diagram for the fertility chip[1]

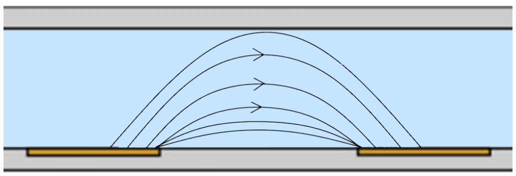

**(a)** Without cells present

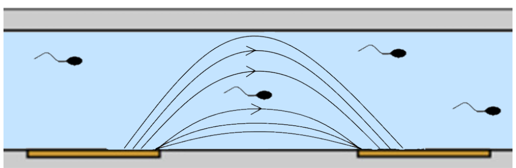

**(b)** With cells present

**Fig. 3** Field lines inside the fertility chip channel (not to scale, adapted from Segerink[5])

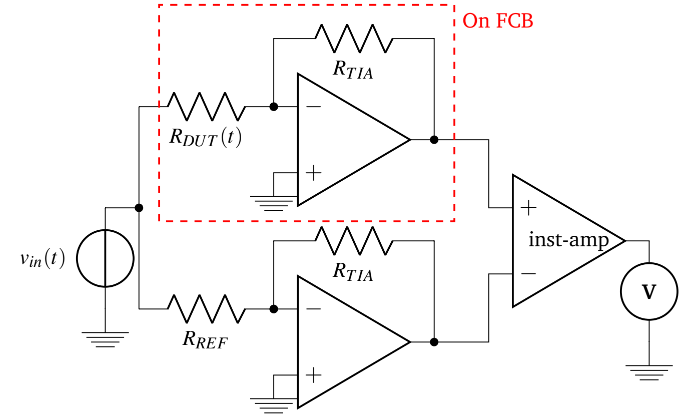


**Fig. 4** Measurement circuit topology to perform differential impedance measurements

a planar electrode configuration and a homogeneous filling with electrolyte. As can be seen, the field lines are denser near the electrodes (the field is non-homogeneous), but they do extend to the top of the channel, meaning that detection is possible in the whole channel. If a cell or insulating bead passes, as depicted in Figure 3b, part of the electric field is shielded, leading to a higher impedance. Because the field is non-homogeneous, the position in the channel where the cell or bead passes affects the response to the passage. However, this is assumed to be a small effect, so it will not be taken into account for the rest of this analysis. Depending on the cell type and whether the cell is alive, the cell behaves like an insulating shell up to $3\,\mathrm{MHz}$[24], after which the cell will start conducting and no effect will be seen.

The expected background impedance can be estimated using the equation for resistance:

$$R = k \cdot \rho \tag{1}$$

in which $k$ is the cell constant and $\rho$ is the resistivity. The cell constant can be determined for planar electrodes using equations given by Olthuis et al[25]. For electrodes with a length of $18\,\mu\mathrm{m}$, width of $20\,\mu\mathrm{m}$ and spacing between the electrodes of $30\,\mu\mathrm{m}$ these give a cell constant of approximately $37.8 \times 10^3\,\mathrm{m}^{-1}$. With an electrolyte with a conductivity of $1.4\,\mathrm{S\,m}^{-1}$, this leads to a resistance of $26.989\,\mathrm{k\Omega}$ ($R_{el}$). The impedance of the double layer capacitance (which ranges from $10\,\mu\mathrm{F\,cm}^{-2}$ to $20\,\mu\mathrm{F\,cm}^{-2}$[5]), ranges from $10.5\,\mathrm{k\Omega}$ to $21\,\mathrm{k\Omega}$ for this configuration at the measurement frequency of $100\,\mathrm{kHz}$. Therefore, the background impedance is expected to be about $60\,\mathrm{k\Omega}$. This is in the same order of magnitude as the impedance measured by Segerink et al[1], which is about $80\,\mathrm{k\Omega}$.

In order to find the impedance *change* for beads with a certain volume, the Maxwell mixing theory can be used[26]. When a particle is present in the electrolyte, the resistance changes:

$$R_{el+b} = R_{el} \cdot \frac{2\sigma_{el} + \sigma_b + \Phi(\sigma_{el} - \sigma_b)}{2\sigma_{el} + \sigma_b - 2\Phi(\sigma_{el} - \sigma_b)} \tag{2}$$

in which $\sigma_{el}$ the conductivity of the electrolyte, $\sigma_b$ the conductivity of the bead and $\Phi$ the volume fraction of the bead. When using a realistic value for the conductivity of polystyrene ($3 \times 10^{-25}\,\mathrm{S\,m}^{-1}$[27]), the resistance changes to $27.017\,\mathrm{k\Omega}$. This means that the resistance difference will be about $28\,\Omega$, or about 0.5‰ for $6\,\mu\mathrm{m}$ beads. For boar spermatozoa with a volume of about $10\,\mathrm{fL}$[28], this results in a resistance change to $27.009\,\mathrm{k\Omega}$, meaning that the resistance difference will be $20\,\Omega$ or 0.33‰.

### 2.3 Electronics

The input Analog to Digital Converter (ADC) of the impedance spectroscope has a resolution of 12 bits. This means, that if the base resistance of the electrolyte would exactly cover the input range of the ADC, the minimal change possible to detect would be $\frac{80{,}000}{2^{12}} \approx 19.5\Omega$. Therefore, a passing sperm cell would only cause 1 bit to change. Also, it would not be possible to differentiate between a bead and a cell, as these lead to the same measurement.

To make optimal use of the dynamic range of the impedance spectroscope, it is worthwhile to make sure only the wanted signal is present at the input. In this case, that means that the background resistance of the electrolyte should be cancelled out. The best way to do that, is by using the electrolyte in another channel on the same chip as the reference electrode. The measured impedance will inherently be the same, meaning that all kinds of drift due to e.g. temperature change and phase shift due to reactive behaviour will also be cancelled out. This will be referred to as 'full differential measurement'. One should, however, pay attention to the concentration of sperm cells present. If this is too

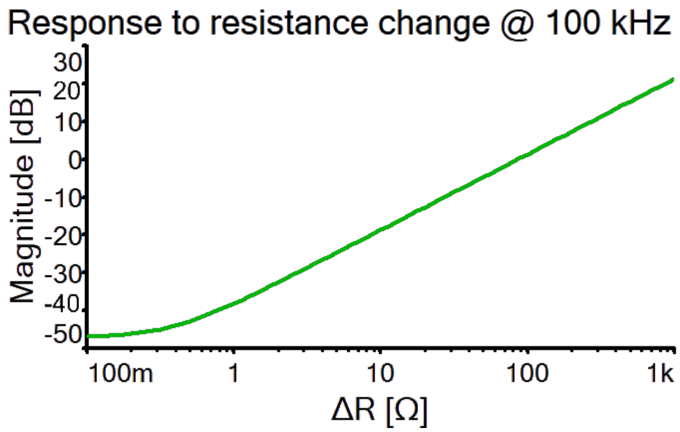


**Fig. 5** Simulation of the circuit response, showing the response of the measurement circuit to a changing resistance added to a base resistance of 80 kΩ

high, the probability of two cells passing the electrodes in both channels at the same time is high, meaning that a reliable measurement is no longer possible. If this is kept low enough, this should not be a problem.

In order to achieve the differential measurement some electronics topologies have been designed. More information, simulations and a comparison can be found in the Supplementary Information: SI.1. The chosen topology using an instrumentation amplifier will be treated here.

In this topology, the full differential measurement is not implemented because the part of the circuit to be integrated on the FCB does not fit within the space constraints. This means that the solution presented will not lead to the best cancellation of the background resistance. It will, however, still lead to a substantial improvement with respect to the non-differential measurement because the output signal will be more optimal for the input range of the impedance spectroscope. See Figure 4, in which $R_{DUT}(t)$ is the impedance of the fertility chip, $R_{REF}$ is a (fixed) reference resistance of about the same value as the background impedance at the target frequency, $R_{TIA}$ is the feedback resistor for each TIA, chosen to be equal, and *inst-amp* is an instrumentation amplifier to determine the difference between the output potential of the two TIAs, which can then be sensed. This way, only the difference in resistance will result in a measurement potential at the output of the instrumentation amplifier, meaning that the full dynamic range of the lock-in amplifier can be used.

To find out the optimal component values for the topology, the circuit has been simulated using National Instruments (NI) Multisim 14.1. A parameter sweep simulation has been set up, to vary the resistance indicated as $R_{DUT}(t)$ in Figure 4 from 0.1 Ω to 1 kΩ, added to a fixed baseline resistor of 80 kΩ. For 20 points per decade, the response of the system is simulated and plotted in Figure 5. The simulations are taken at a constant frequency of 100 kHz, with an excitation potential of 2Vpp (taken as an example, should be representative for all excitation potentials). As can be found in this graph, the system starts working linearly from a resistance difference of 0.5 Ω up to 1 kΩ, which means that it should be able to detect the resistance differences as calculated. Below

**(a)** Reservoir **(b)** Flow sensor **(c)** Output

**Fig. 6** Sample MFBBs made by Dekker et al[29]

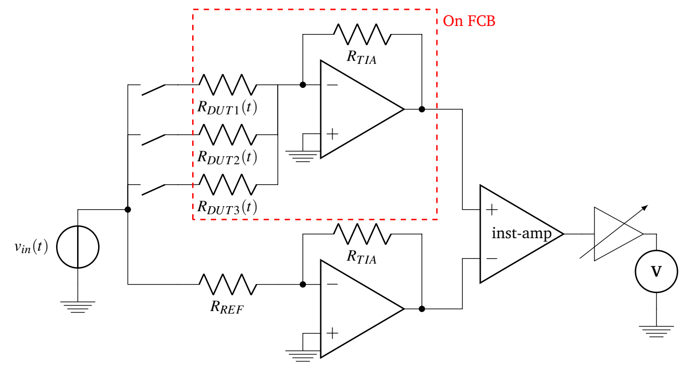


**Fig. 7** Full measurement circuit, including additional gain and switchable channel selection

0.5 Ω a response is visible, but it is not linear. As can be seen in the additional simulations done in the Supplementary Information: SI.1, this behaviour is dependent on frequency, leading to think that the bandwidth of one of the amplifiers would be the limiting factor.

In order to broaden the range of applications, additional gain could be needed. Preferably, this can be configured without the need to (de)solder a component. Therefore, a variable gain amplifier is included in the final design, which can be set to a gain of 1 to 100 times using DIP-switches. Another consideration is how to select which channel on the fertility chip is used as the measurement channel. Preferably, this can also be configured without (de)soldering. In the design, this is also implemented using DIP-switches. For the full functional design of the electrical part of the system, see Figure 7. In this figure, each channel on the fertility chip is shown as an impedance, called $R_{DUTn}(t)$ with n from 1 to 3. The design uses a card edge connector to connect the FCB to the rest of the system. More information on the implementation of the non-FCB electronics can be found in the Supplementary Information: SI.3.

### 2.4 Microfluidics

In order to introduce a sample to the fertility chip and read out the electronics, an FCB has been designed. The electrodes on the fertility chip can be interfaced using spring loaded probes, which will press onto the contact pads (located at the same side of the fertility chip as the fluidic connections). These are connected to

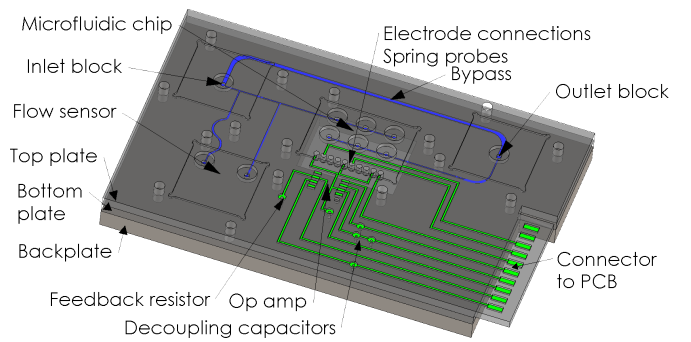


**Fig. 8** FCB design, showing the microfluidic connections (in blue) and the first TIA (in green). The dimensions are 85 by 54 mm.

the rest of the electronics by the use of conductive paste. Since the resulting current through the fertility chip will be small (about $200\,\mu$A or lower), therefore prone to noise, it is critical to detect this current as close to the fertility chip as possible. Therefore, a TIA to convert the current to a potential difference is integrated on the FCB, marked as 'On FCB' in Figure 4. For more information about the FCB design, see Supplementary Information: SI.2.

In the research done by Dekker et al[29], some MFBBs have been developed:

- A reservoir which can be attached to a pressure pump, to induce a flow in the system, see Figure 6a;
- A differential flow sensor, see Figure 6b;
- A simple block to transport liquid to a waste reservoir, see Figure 6c.

These MFBBs can be used to introduce a sample to the fertility chip and measure the flow going through it. To keep the dead volume small, the connecting fluidic channels should be as small as possible, without risking a blockage. Therefore, their dimensions are chosen to be $200\,\mu$m for the depth and the width, as this is the smallest mill available and blockage is not a risk for this dimension. The available flow sensor has a measurement range of $0\,\mu$L min$^{-1}$ to $100\,\mu$L min$^{-1}$, but the fertility chip was only used with a maximum of $0.1\,\mu$L min$^{-1}$. In order to regulate the flow going through the fertility chip to a level detectable by the flow sensor, a bypass has been added. The fertility chip will receive 1.2 ‰ of the total flow (determined by calculating the hydrodynamic resistances of the different paths[30]), meaning that the flow range (maximum of $83\,\mu$L min$^{-1}$) will be in accordance with the measurement range of the flow sensor.

The microfluidic in- and outlets of a MFBB are connected to the FCB by using O-rings with an outer diameter of 3.6 mm and inner diameter of 1.2 mm at the interface, to prevent leakage. Similarly, if an in or outlet is not to be used, it can be closed using a blocking element of the same outer diameter as the O-ring, but without the hole in the middle. In order for these solutions to work, a mechanical pressure must be applied to the MFBB to close the interface between O-ring/blocker and MFBB/FCB. This can be done by utilizing a clamp, which can be screwed on the backplate of the FCB. For the existing MFBBs, existing clamps for 15x15mm

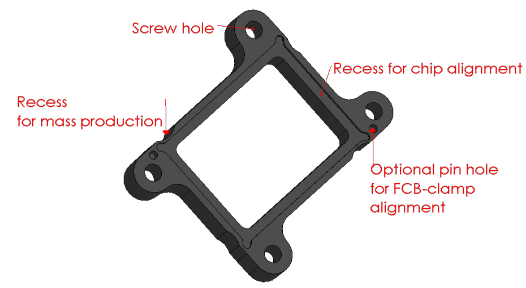


**Fig. 9** Clamp design for the fertility chip of 15 by 20 mm

blocks could be used. For the fertility chip, however, a custom clamp must be used as the dimensions are 20 by 15 mm. See Figure 9 for the design of this clamp, more information can be found in Supplementary Information: SI.4.

## 3 Materials & Methods

### 3.1 Electrode material

In order to interface the fertility chip and make an electric circuit on the FCB, a conductive paste will be used. Two of those were available, one with carbon graphite as a conductive element (Gwent Electronic Materials, C2000802P2) and the other with silver/silver chloride as a conductive element (Gwent Electronic Materials, C2051014P10). An experiment has been devised with a credit-card sized (85x54mm), 1 mm thick wafer (Topas grade 6013, Denz BIO-Medical, Austria) of Cyclo Olefin Copolymer (COC) on which channels are milled with a variety of dimensions, in which the paste can be applied and cured. Using an Agilent 34401A multimeter in resistance mode and two measurement probes, the resistivity will be characterized. For more information on the pastes, see Supplementary Information: SI.6.

### 3.2 Fabrication

The design for the FCB was made in SOLIDWORKS 2017 and exported to milling instructions using Autodesk HSMWorks 2018. These can be used to produce the FCB using a Sherline milling machine and a PC with LinuxCNC, starting with a 2mm thick credit-card sized COC substrate. For more information about micromilling, see Supplementary Information: SI.5. See Figure 10 for a schematic overview of the fabrication process. After milling the substrate on both sides, the conductive paste will be applied around the spring probe locations and the spring probes (Smiths Connectors, 101582) will be inserted. After curing the paste, another 2mm thick credit-card sized COC substrate will be bonded to this side using solvent bonding, sealing the channels. Subsequently, the last holes will be drilled and some substrate will be removed in order to accommodate the card edge connector. Then the rest of the paste will be applied and two decoupling capacitors, two pin headers for the feedback resistor and the op amp IC will be inserted. After curing, the FCB will be ready to be used. For a full description of the fabrication process, see Supplementary Information: SI.7.

The baseplate for the FCB has been exported to milling instruction using Autodesk HSMWorks 2018 as well, to be produced us-

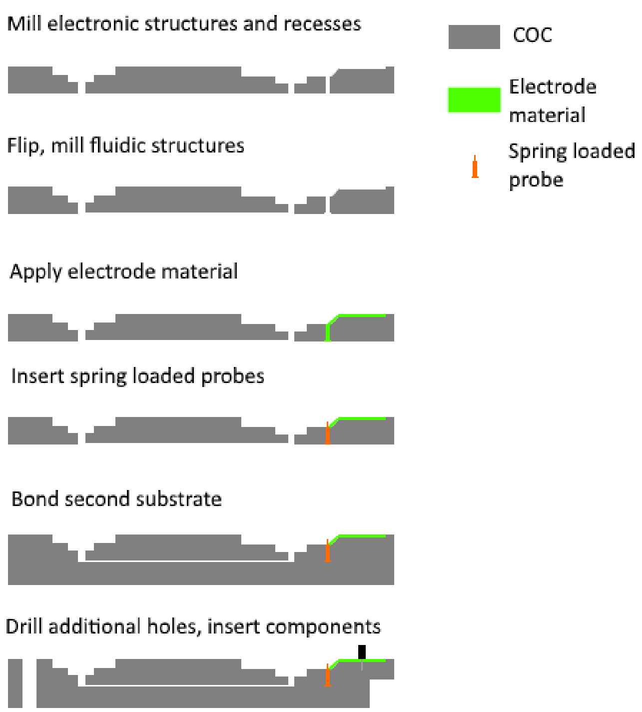


**Fig. 10** Schematic overview of the fabrication process for the FCB

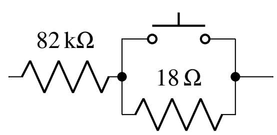


**Fig. 11** Circuit to test circuit response to a small resistance change

ing the same machine as the FCB, out of aluminium. After opening the window at the location of the fertility chip for easy optical access and drilling the holes, the holes will be threaded to be able to mount the FCB and clamps on the baseplate.

For the fertility chip, a clamp was needed. The design for the clamp was exported to an STL file and can be manufactured using 3D-printing based on a stereolithographic technique (Formlabs Form 2). For more information about stereolithography, see Supplementary Information: SI.5.

### 3.3 Electric validation

In order to validate the working of the electronics, a resistance test has been set up. On the FCB, a fixed resistance will be mounted of about 82 kΩ instead of the fertility chip. The feedback resistor for the TIA on the FCB will also be about 82 kΩ. The circuit in Figure 11 will replace the reference resistor $R_{REF}$ in Figure 4. If the button is pressed, the total resistance will decrease with an amount of 18 Ω, which has the same effect as an increase of this amount in $R_{DUT}$. This way, the effect on the measurement of a resistance change can be investigated. The measurement frequency to be used will be 100 kHz, and the actuation potential difference will be 0.3 VRMS.

### 3.4 Fluidic validation

For validating the working of the system for its final purpose, a test using beads has been set up. A suspension of 6 $\mu$m diameter dyed red beads (Polysciences Inc, 15714) with a concentration of $10^6$ mL$^{-1}$ in Phosphate Buffered Saline (PBS) (Sigma Aldrich, P4417-100TAB) will be introduced to the system. This is done using the MFBBs described in subsection 2.4, mounted on the FCB using the mentioned clamps, O-rings (Eriks BV, AS568-002) and blocking elements (which can be fabricated using PDMS and a mould). A Fluigent MFCS-4C pressure pump will be used to push the solution through the system.

## 4 Results & Discussion

### 4.1 Electrode material

When looking closely at the substrates, of which pictures can be found in Supplementary Information: SI.6, some of the channels on the carbon graphite plate contain holes, caused by some of the paste being removed out of the channel by the windscreen wiper. The silver/silver chloride substrate doesn't seem to suffer that much from this problem. The results can be found in Figure 12 for the carbon graphite paste and Figure 13 for the silver/silver chloride paste. As can be seen, the resistance of the carbon graphite channels is much higher than the resistance of the silver/silver chloride channels. Furthermore, some of the carbon graphite channels have a much higher resistance than would be expected, which can be explained by the holes mentioned previously. Based on these results, the paste based on silver/silver chloride will be used as electrode material.

### 4.2 Fabrication

The FCB and additional electronics have been fabricated, see Figure 14. Some dimensions have been measured to verify the design to product workflow. For a measurement of the fluidic channels, see Figure 15a and Figure 15b. The designed channel width is 200 $\mu$m for the main channels, leading to a deviation of 62.3% for the top channel and 37.0% for the bottom channel. The designed bypass width is 800 $\mu$m, leading to a negative deviation of

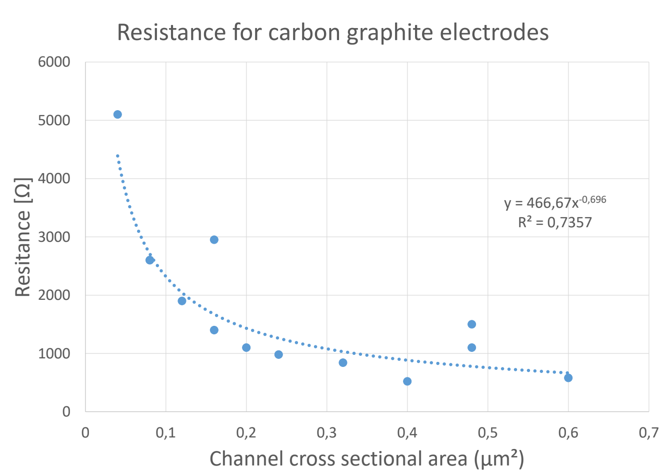


**Fig. 12** Resistance vs channel volume for carbon graphite electrodes

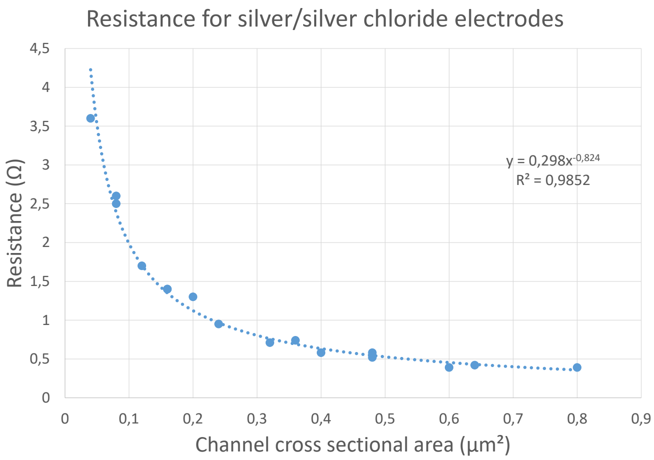


**Fig. 13** Resistance vs channel volume for silver/silver chloride electrodes

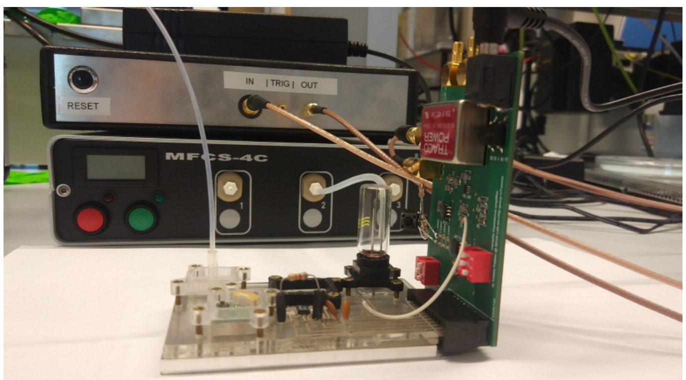


**Fig. 14** Overview of the whole system

33.7%. Revisiting the calculations in subsection 2.4, the fertility chip will receive 2.08‰ of the total flow, meaning that the total flow will have a maximum of $48.2\,\mu\mathrm{L\,min^{-1}}$, limiting the dynamic range of the flow sensor.

For a measurement of the clamp side, see Figure 15c. The designed top dimension is $800\,\mu$m and the total dimension is $1930\,\mu$m, leading to a deviation of 6.5% and 2.5%, respectively. Deviations in this part could lead to a MFBB not fitting inside the clamp, which could lead to problems mounting the MFBB and, possibly, breaking of the MFBB. However, the deviations found are perfectly fine for this use. For a measurement of two holes in the clamp, see Figure 15d. The designed diameter of the small hole is $1000\,\mu$m and of the large hole is $2100\,\mu$m, leading to a deviation of 15.4% and 2.1%, respectively. Deviations in the holes could lead to screws not perfectly fitting, and a loose clamping. However, through the countersunk design, a very large deviation is required to cause problems, which is not the case. Finally, for a measurement of an electrode channel on the FCB, see Figure 15e. The designed electrode width is $400\,\mu$m, leading to a deviation of 3.25%.

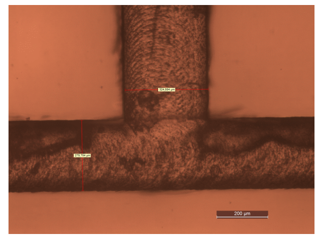

**(a)** At channel junction, top=$324.6\,\mu$m, bottom=$275.8\,\mu$m

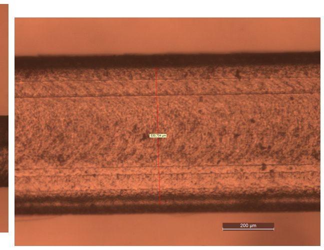

**(b)** At bypass, width=$530.7\,\mu$m

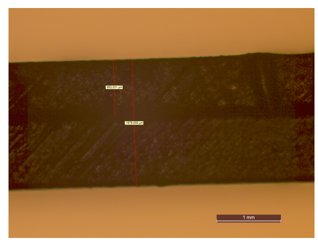

**(c)** At side of clamp, top=$852\,\mu$m, total=$1979\,\mu$m

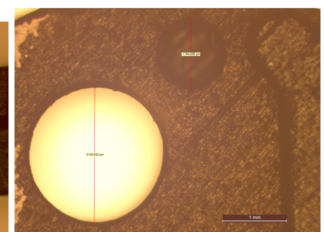

**(d)** At holes in clamp, large hole=$2145\,\mu$m, small hole=$1154\,\mu$m

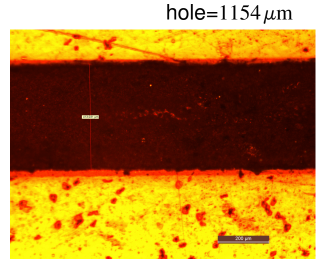

**(e)** At electrode, width=$413\,\mu$m

**Fig. 15** Measurements of fabricated elements made using a microscope

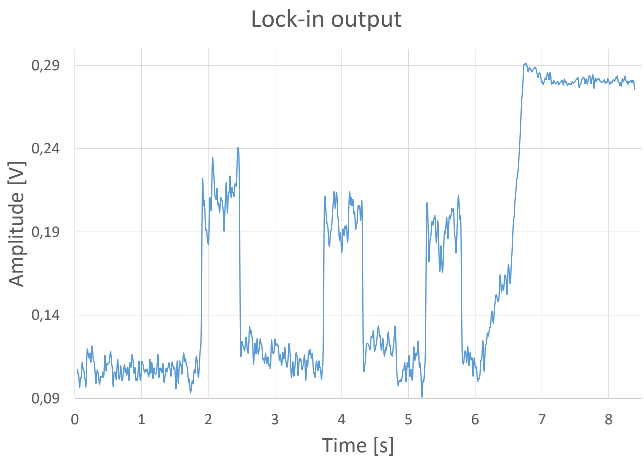


**Fig. 16** Results for the electric validation, in which the button was pressed three times

### 4.3 Electric validation

The set-up as described in subsection 3.3 has been built and used to validate the electric functionality. The filter settings of the lock-in amplifier were set to their default settings, and the additional gain amplifier was set to 5x. The results are plotted in Figure 16. Some observations can be made: the button has been pressed three times, which is clearly visible. The amplitude difference for the small resistance change is substantial, about 100 mV, which is a change of about 200 ADC levels, and consistent. The signal is very noisy, from 20 mV to 55 mV, which is a difference of about 40 to 110 ADC levels. The system is also susceptible to external factors, which is clearly visible in the graph. At sample 2800, the hand of the person pressing the button was pulled away from the set-up, leading to a major increase in signal. However, the button press responses are clear enough to say we can reliably detect a resistance change of 18 Ω.

### 4.4 Fluidic validation

Because of time constraints, no fluidic testing was carried out.

## 5 Conclusions & Recommendations

Some very promising results have been acquired:

1. Integrating electrodes and even some electric components on an FCB is very well possible by using conductive paste;

2. Stereolithography can be used as a rapid production method for MFBB clamps;

3. It is shown that a resistance difference of 18 Ω can be detected on top of a 82 kΩ background;

Based on the results given above, the system is a promising set-up which can be used to get the fertility chip system towards a production-ready PoC prototype, which is the next step for the fertility chip on the way to market.

Next steps to be taken to get towards a complete solution, besides the recommendations made in section SI.2 and section SI.3, are:

1. Integrate a mixer MFBB to perform auto-calibration using both microfluidic beads and a sperm sample. Because we can differentiate between beads and spermatozoa, it is possible to relate the concentration of sperm cells to the concentration of beads and number of beads and spermatozoa counted in a certain amount of time. This could be done by extending the size of the FCB to accommodate two more MFBBs: the mixer and another reservoir for the calibration fluid;

2. Implement a full differential measurement using another channel of the fertility chip, in order to cancel the thermal drift and phase shifts present in the impedance of the fertility chip. This could be done by finding a way to integrate more electronics on the FCB, or by moving the measurement area to a place close to the connection of the rest of the system, delegating the conversion of the currents and the differential measurement;

3. Use the flow sensor as a feedback system to regulate the pressure pump to the wanted flow rate. This means that no longer a pressure has to be set, but a flow can be set as well;

4. Because it is very hard to mount the fertility chip without breaking it, the clamp design should be adjusted so it applies pressure on the chip (to close the O-rings), but then touches the FCB to prevent breakage;

5. The headers used for the connection of the feedback resistor on the FCB are prone to breaking, so if no changing is required these should be replaced by a permanent resistor. To do this, the hole diameters need to be adjusted accordingly.

## Acknowledgements

This work was supported by ENIAC Joint Undertaking (JU), a public-private partnership focusing on nanoelectronics that brings together ENIAC Member/Associated States, the European Commission, and AENEAS (an association representing European R&D actors in this field).

The author wishes to express his gratitude to J. Loessberg-Zahl for fabricating the clamps for the fertility chip, and to F. van den Brink for brainstorming about the electrode material.

## References

1 L. I. Segerink, A. J. Sprenkels, P. M. ter Braak, I. Vermes and A. van den Berg, *Lab Chip*, 2010, **10**, 1018–1024.
2 M. J. Leene, *Thesis*, University of Twente, 2016.
3 E. Hoogendijk, *BSc-thesis*, University of Twente, 2016.
4 L. R. Volpatti and A. K. Yetisen, *Trends Biotechnol.*, 2014, **32**, 347–350.
5 L. I. Segerink, *PhD-thesis*, University of Twente, 2011.
6 J. Sun, J. Yang, Y. Gao, D. Xu and D. Li, *Microfluid. Nanofluidics*, 2017, **21**, 33.
7 F. Liu, Y. Han, L. Du, P. Huang and J. Zhe, *Microfluid. Nanofluidics*, 2016, **20**, 27.
8 Z. Mei, Z. Liu and Z. Zhou, *AIMS Biophys.*, 2016, **3**, 596–608.

9 Y. Chen, J. Guo, H. Muhammad, Y. Kang and S. K. Ary, *IEEE Trans. Biomed. Eng.*, 2016, **63**, 311–315.

10 G. Ferrari, M. Carminati, G. Gervasoni, M. Sampietro, E. Prati, C. Pennetta, F. Lezzi and D. Pisignano, 2015 Int. Conf. Noise Fluctuations, 2015, pp. 1–6.

11 M. Jalali, A. Nabavi, M. Moravvej-Farshi and A. Fotowat-Ahmady, *Microelectronics J.*, 2008, **39**, 1843–1851.

12 M. Crescentini, M. Bennati, S. Saha, J. Ivica, M. de Planque, H. Morgan and M. Tartagni, *Sensors*, 2016, **16**, 709.

13 M. Kubo, H. Yotsuda, T. Kosaka and N. Nakano, 2015 Int. Symp. Intell. Signal Process. Commun. Syst., 2015, pp. 307–311.

14 J. H. Scofield, *Am. J. Phys.*, 1994, **62**, 129–133.

15 M. Carminati, G. Gervasoni, M. Sampietro and G. Ferrari, *Rev. Sci. Instrum.*, 2016, **87**, 026102.

16 D. Mark, S. Haeberle, G. Roth, F. von Stetten and R. Zengerle, *Chem. Soc. Rev.*, 2010, **39**, 1153.

17 A. Wu, L. Wang, E. Jensen, R. Mathies and B. Boser, *Lab Chip*, 2010, **10**, 519–521.

18 J. Ducrée, S. Haeberle, S. Lutz, S. Pausch, F. V. Stetten and R. Zengerle, *J. Micromechanics Microengineering*, 2007, **17**, S103–S115.

19 R. Sista, Z. Hua, P. Thwar, A. Sudarsan, V. Srinivasan, A. Eckhardt, M. Pollack and V. Pamula, *Lab Chip*, 2008, **8**, 2091.

20 A. K. Yetisen, M. S. Akram and C. R. Lowe, *Lab Chip*, 2013, **13**, 2210.

21 H. van Heeren, T. Atkins, N. Verplanck, C. Peponnet, P. Hewkin, M. Blom, W. Buesink, J.-E. Bullema and S. Dekker, 2016, DOI: 10.13140/RG.2.1.1698.5206.

22 H. van Heeren, T. Atkins, N. Verplanck, C. Peponnet, P. Hewkin, M. Blom, W. Buesink, J.-E. Bullema and S. Dekker, 2016, DOI: 10.13140/RG.2.1.3318.9364.

23 V. Gubala, L. F. Harris, A. J. Ricco, M. X. Tan and D. E. Williams, *Anal. Chem.*, 2012, **84**, 487–515.

24 H. Morgan, T. Sun, D. Holmes, S. Gawad and N. G. Green, *J. Phys. D. Appl. Phys.*, 2007, **40**, 61–70.

25 W. Olthuis, W. Streekstra and P. Bergveld, *Sensors Actuators B Chem.*, 1995, **24**, 252–256.

26 T. Sun, C. Bernabini and H. Morgan, *Langmuir*, 2010, **26**, 3821–3828.

27 V. Adamec, *Kolloid-Zeitschrift Zeitschrift für Polym.*, 1970, **237**, 219–229.

28 A. M. Petrunkina, M. Hebel, D. Waberski, K. F. Weitze and E. Topfer-Petersen, *Reproduction*, 2004, **127**, 105–115.

29 S. Dekker, A. van den Berg and M. Odijk, 2017, DOI: unpublished working paper.

30 H. Bruus, *Theoretical Microfluidics*, Oxford University Press, 2008.

31 Zurich Instruments, *HF2 user manual - ziControl edition*, 2015, `https://www.zhinst.com/sites/default/files/ziHF2{_}UserManual{_}ziControl{_}45800.pdf`.

32 J. O. P. Zanen, *Datasheet differential source- measurement unit for resistance difference measurements*, University of twente technical report, 2016.

33 B. van Dam and W. Buesink, 2017, DOI: unpublished working document.

34 J. G. Bomer, K. Vermeul, P. M. ter Braak, L. de Vreede, M. Odijk, S. Dekker and F. van den Brink, *Rapid prototyping manual*, 2017.

SUPPLEMENTARY INFORMATION

## SI.1 Clarification of Electronics design

In the original work by Segerink[1], a home-made impedance spectroscope was used to detect the impedance, which worked using a pick-up amplifier and synchronous detection. Later on, other home-made circuits (see for example Figure 17)[2] and an impedance spectroscope made by Zurich Instruments (see Figure 18)[3] have been used. These solutions were all based on detecting the whole impedance, and detecting the peaks afterwards. This means that only a small part of the whole dynamic range of the final ADC could be used for peak detection, leading to loss of precision.

To improve the detection of small variations in impedance, a couple of topologies are proposed, namely using a differential driver, a summing amplifier, an instrumentation amplifier and an inverting amplifier. These will be analyzed and simulated piece by piece, after which a comparison and conclusion will be given. All the simulations have been carried out by NI Multisim 14.1.

### SI.1.1 Differential Driver

This topology, as depicted in Figure 19, is inspired by the design as proposed by Zanen[32]. The main idea is to create a signal and its inverse based on an input sine signal, then feed it to both the device and a resistance in the same order of magnitude as the background electrolyte impedance. After these resistances, a node sums both currents to only keep the difference (which contains the impedance difference and therefore the signal), which is then converted to a voltage by the TIA. The impedance difference

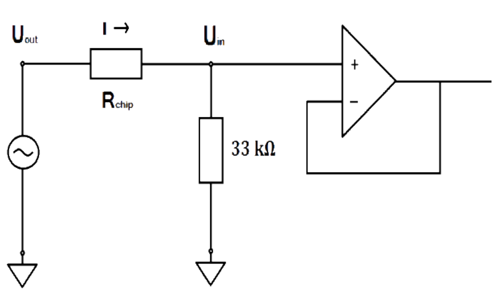


**Fig. 17** One of the used home-made measurement circuits[3]

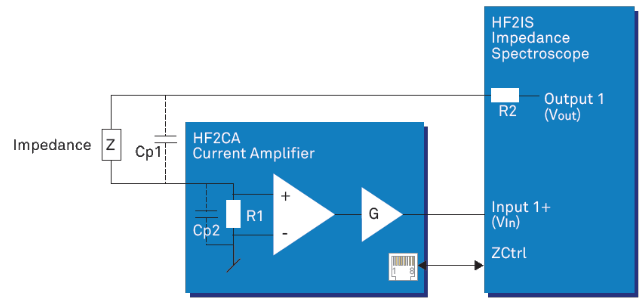


**Fig. 18** The measurement circuit using the Zurich Impedance Spectroscope[31]

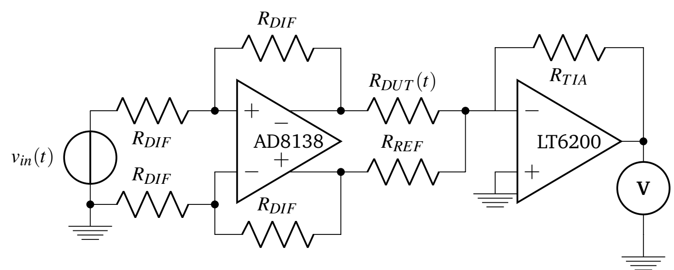


**Fig. 19** Measurement circuit, based on differential driver

can then be determined:

$$R_{DUT}(t) = R_{base} + \Delta R(t)$$

$$R_{REF} = R_{base}$$

$$u_{DUT} = -u_{in}$$

$$u_{REF} = u_{in}$$

$$u_{out}(t) = i_{TIA}(t) \cdot R_{TIA}$$

$$i_{TIA}(t) = i_{REF} + i_{DUT}(t) = \frac{u_{in}}{R_{base}} + \frac{-u_{in}}{R_{base} + \Delta R(t)}$$

$$u_{out}(t) = \frac{-u_{in} \cdot R_{TIA} \cdot \Delta R(t)}{R_{base}^2 + R_{base} \cdot \Delta R(t)}$$

$$\Delta R(t) = \frac{-R_{base}}{1 + \frac{u_{in} \cdot R_{TIA}}{u_{out}(t) \cdot R_{base}}}$$

The circuit has been simulated, using the following values: $R_{DIF} = 470\Omega, R_{REF} = 80k\Omega, R_{TIA} = 3.3k\Omega$ and varying $R_{DUT}$ from 0.1 Ω to 1 kΩ with a baseline of 80 kΩ, yielding the results in Figure 20. As can be seen in this figure, the circuit starts to change output at a resistance difference of about 10 Ω, and is linear from 300 Ω up to 1 kΩ.

### SI.1.2 Summing amplifier

This topology, as depicted in Figure 21, is inspired by the fact that, for an $R_{TIA}$ equal to the background electrolyte impedance, the output of the TIA should be the same as the inverse input

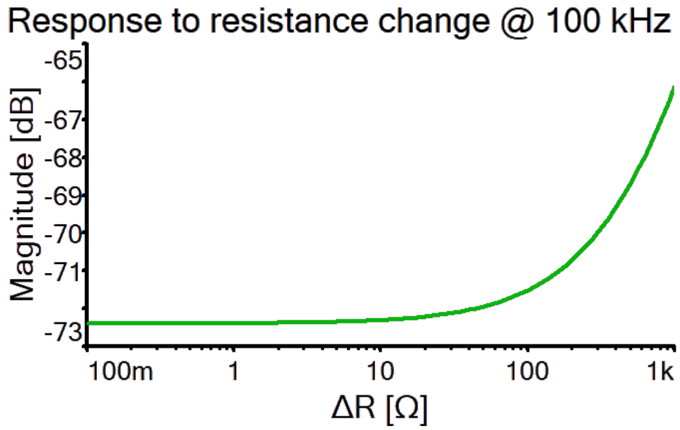


**Fig. 20** Simulation for the differential driver circuit

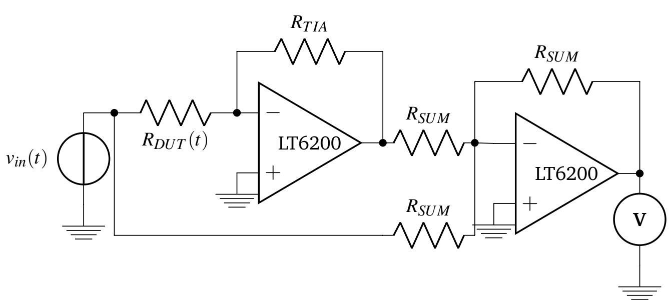


**Fig. 21** Measurement circuit, based on summing amplifier

voltage:

$$U_{out} = -R_{TIA} \cdot I_{in} \tag{3}$$

$$I_{in} = U_{in} \cdot R_{dut}(t) \tag{4}$$

if $R_{TIA} = R_{dut}(t)$:

$$U_{out} = -U_{in} \tag{5}$$

We can then use a summing amplifier to subtract the input signal from the background electrolyte impedance signal, which then leaves the difference signal.

The circuit has been simulated, using the following values: $R_{SUM} = 1k\Omega, R_{TIA} = 80k\Omega$ and varying $R_{DUT}$ from $0.1\,\Omega$ to $1\,\mathrm{k}\Omega$ with a baseline of $80\,\mathrm{k}\Omega$, yielding the results in Figure 22. As can be seen in this figure, the circuit starts to change output at a resistance difference of about $10\,\Omega$, and is linear from $400\,\Omega$ up to $1\,\mathrm{k}\Omega$.

### SI.1.3 Instrumentation amplifier

For this topology, as depicted in Figure 23, the TIA as depicted in Figure 1 is duplicated with a fixed reference resistance (in the same order of magnitude of the background electrolyte resistance), after which the output voltages are fed into an instrumentation amplifier. An instrumentation amplifier is a difference amplifier, with the characteristic that no impedance matching between the inputs is needed because of the high-impedance input buffers and the gain can be tuned very easily. It is therefore very suited for use in measurement equipment, also due to its low drift and low noise. In this topology, it determines the difference between the inputs and amplifies it. This topology can also be used to reduce the noise in the conductance signal[15].

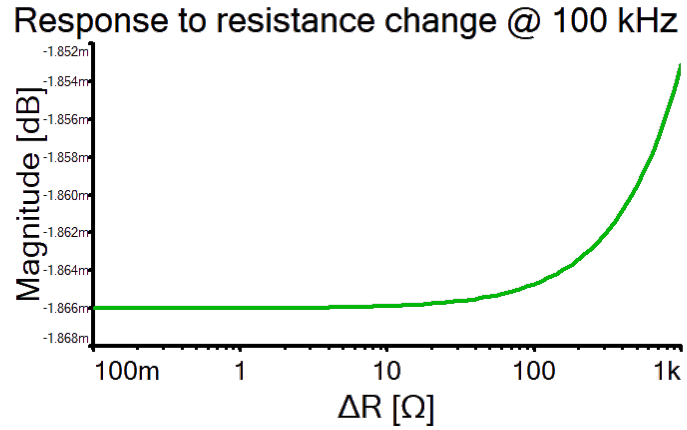


**Fig. 22** Simulation for the summing amplifier circuit

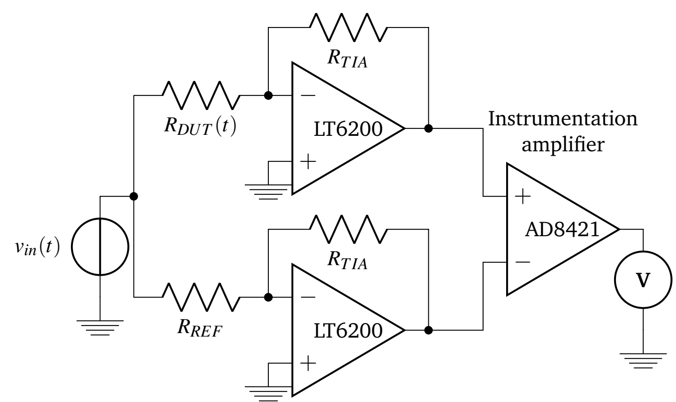


**Fig. 23** Measurement circuit, based on instrumentation amplifier

The circuit has been simulated, using the following values: $R_{REF} = 80k\Omega, R_{TIA} = 80k\Omega$ and varying $R_{DUT}$ from $0.1\,\Omega$ to $1\,\mathrm{k}\Omega$ with a baseline of $80\,\mathrm{k}\Omega$, yielding the results in Figure 24. As can be seen in this figure, the circuit starts to change output at a resistance difference below $100\,\mathrm{m}\Omega$, and is linear from $0.5\,\Omega$ up to $1\,\mathrm{k}\Omega$.

### SI.1.4 Inverting amplifier

This implementation, as depicted in Figure 25, follows the same inspiration as the differential driver topology, but uses a different way to generate the inverted input signal. This is done by using an inverting amplifier with amplification -1, which then drives the reference resistance. After this, the currents are again added to keep the difference between them, and converted to a voltage using the TIA.

The circuit has been simulated, using the following values: $R_{INV} = 100\Omega, R_{REF} = 80k\Omega, R_{TIA} = 80k\Omega$ and varying $R_{DUT}$ from $0.1\,\Omega$ to $1\,\mathrm{k}\Omega$ with a baseline of $80\,\mathrm{k}\Omega$, yielding the results in Figure 26. As can be seen in this figure, the circuit starts to change

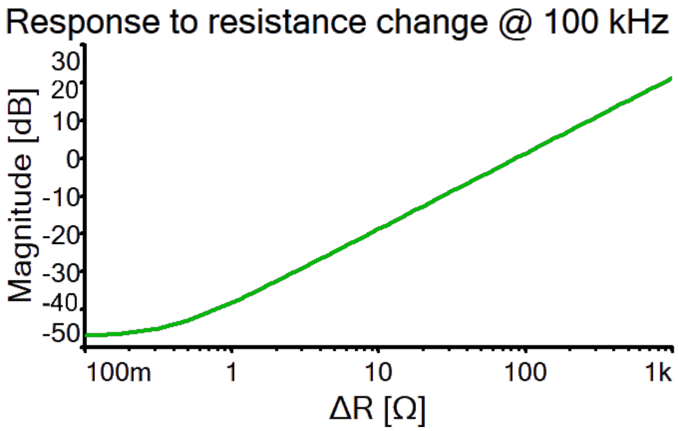


**Fig. 24** Simulation for the instrumentation amplifier circuit

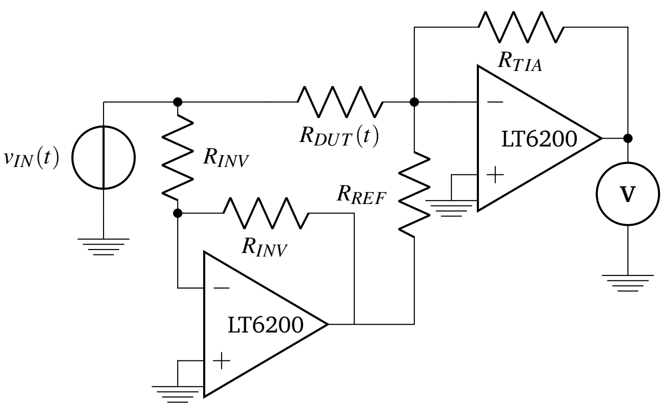


**Fig. 25** Measurement circuit, based on inverting amplifier

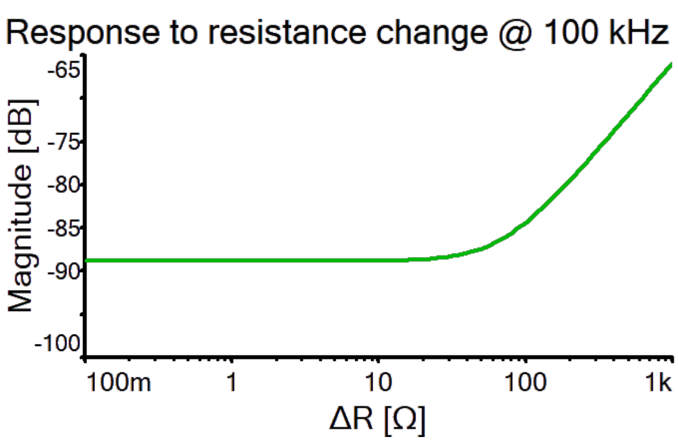


**Fig. 26** Simulation for the inverting amplifier circuit

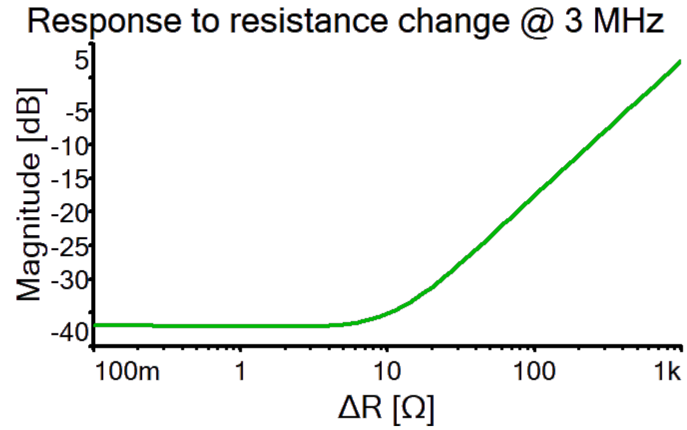


**(a)** At 3 MHz

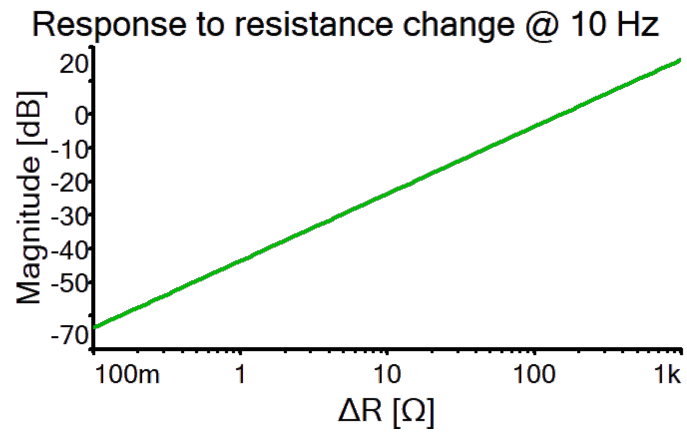


**(b)** At 10 Hz

**Fig. 27** Additional simulations for the instrumentation amplifier circuit

output at a resistance difference of about 10 Ω, and is linear from 100 Ω up to 1 kΩ.

### SI.1.5 Comparison

As can be seen in the previous paragraphs, the output of the differential driver, summing amplifier and inverting amplifier circuits is not behaving linearly in the desired measurement range (Resistance differences of 20 Ω). This means that these circuits are not usable as measurement circuit topology in this project. The instrumentation amplifier circuit, however, performs very well in the desired measurement range. To find out whether it will also perform well in other scenarios, additional simulations at different excitation frequencies have been performed. These can be found in Figure 27. As can be seen, the response degrades for higher frequencies. However, at 3 MHz, we can still determine resistance differences from 20 Ω upwards linearly. Furthermore, for low frequencies the circuit keeps behaving perfectly.

## SI.2 FCB Design

In order to introduce a sample to the fertility chip and read out the electronics, an FCB has been designed. The electrodes on the fertility chip can be interfaced using spring loaded probes (Smiths connectors), which will press onto the contact pads. These are connected to the rest of the electronics by the use of conductive paste. Since the resulting current through the fertility chip will be small, it is critical to detect this current as close to the fertility chip as possible. Therefore, a TIA to convert the current to a potential difference is integrated on the FCB. Furthermore, a bypass to regulate the flow going through the fertility chip to a level detectable by the flow sensor is included. For an exploded view of all included components of the FCB, see Figure 29. For the top view of the FCB design, see Figure 30, for the embedded channel design, see Figure 31, for the design of the backplate (sealing the channels), see Figure 32 and for the design of the baseplate on which the FCB can be mounted see Figure 33. The FCB has been manufactured and assembled, see Figure 34 for a photograph.

### SI.2.1 Electronics

In order to convert the current through the fertility chip to a voltage, a TIA is included on the FCB. The feedback resistance can be changed easily due to the pin headers in which this is mounted. Besides the red part marked 'On FCB' in Figure 4, some power supply decoupling capacitors are included. See Figure 30 for the layout of the circuit on the FCB. The full bill of materials for the FCB can be found in Table 2.

### SI.2.2 Bypass

The bypass is meant to reduce the flow through the fertility chip. The fraction of the flow that will go through the fertility chip can be determined using the equivalent circuit diagram depicted in Figure 28 and determining the various resistances[30]. For rectangular channels:

$$R = \frac{12\eta L}{1-0.63(\frac{h}{w})}\frac{1}{h^3 w} \tag{6}$$

in which $\eta$ the viscosity (1.0016 mPa s for water @ 20 °C), $L$ the length of the channel, $h$ the height of the channel and $w$ the width of the channel. For square channels (width equal to height) goes:

$$R = 28.4\eta L \frac{1}{h^4} \tag{7}$$

Using the values in Table 1, the equal resistance of the part becomes $1.217 \times 10^{14}\,\mathrm{Pa\,s\,m^{-3}}$. Therefore, the ration between the flows becomes 1.24‰, which means that the total flow will become about $80.65\,\mu\mathrm{L\,min^{-1}}$ for a flow of $0.1\,\mu\mathrm{L\,min^{-1}}$ through the fertility chip.

### SI.2.3 Variables

In the SOLIDWORKS model, a couple of variables have been defined in order to make changing the design very easy. For instance, if the inter-electrode spacing needs to be increased be-

**Table 1** Hydrodynamic resistances in FCB

| Resistor | w [$\mu$m] | h [$\mu$m] | L [mm] | Resistance [$10^{11}\,\mathrm{Pa\,s\,m^{-3}}$] |
|---|---|---|---|---|
| FCB1 | 200 | 200 | 29.02 | 5.16 |
| chip1 = chip2 | 96 | 18 | 1.525 | 371 |
| measurement | 38 | 18 | 0.6 | 464 |
| FCB2 | 200 | 200 | 32.5 | 5.78 |
| bypass | 800 | 200 | 67.67 | 1.51 |

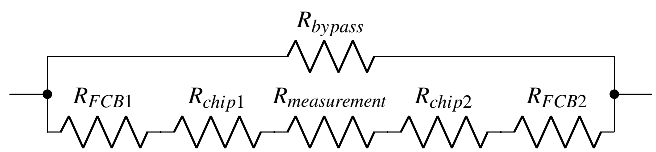


**Fig. 28** Equivalent hydrodynamic circuit diagram of FCB

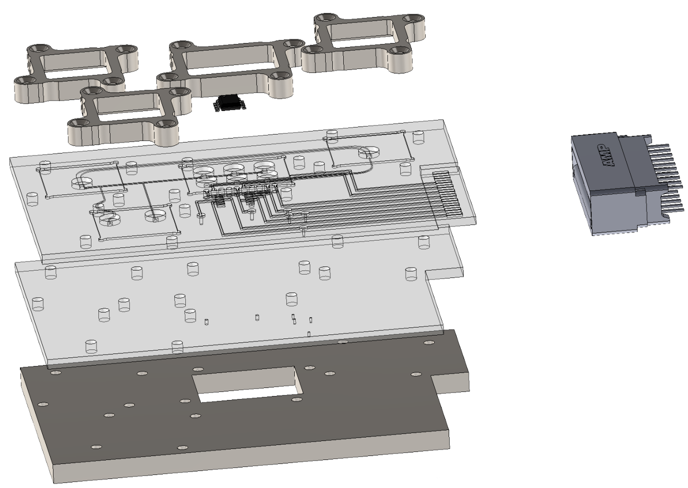

**Fig. 29** An exploded view of all the FCB components

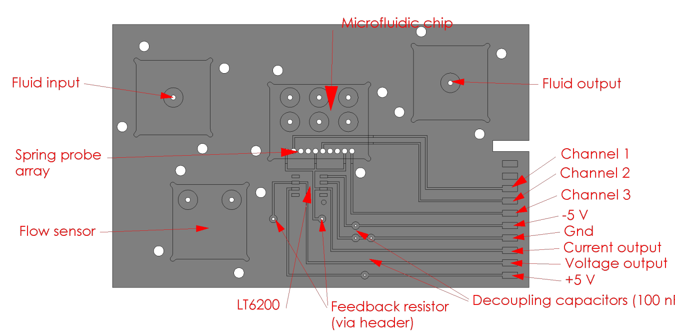


**Fig. 30** The top view of the FCB

**Table 2** Bill of Materials for the FCB

| Quantity | Type of part | Value/part nr | Manufacturer | Farnell order code |
|---|---|---|---|---|
| 1 | Op amp (TIA) | LT6200CS8 | Linear Technology | 1330751 |
| 1 | Female pin header (strip of 10) | n.a. | Multicomp | 1593464 |
| 1 | Resistor (feedback) | 80 kΩ | Multicomp | 9340955 |
| 2 | Capacitor (power decoupling) | 100 nF | Vishay | 1141775 |
| 6 | Spring loaded probe | 101582 | Smiths connectors | n.a. |

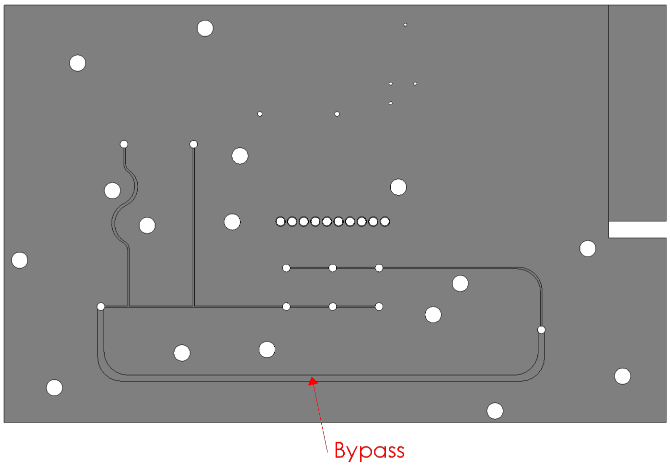


**Fig. 31** The bottom view of the FCB top plate

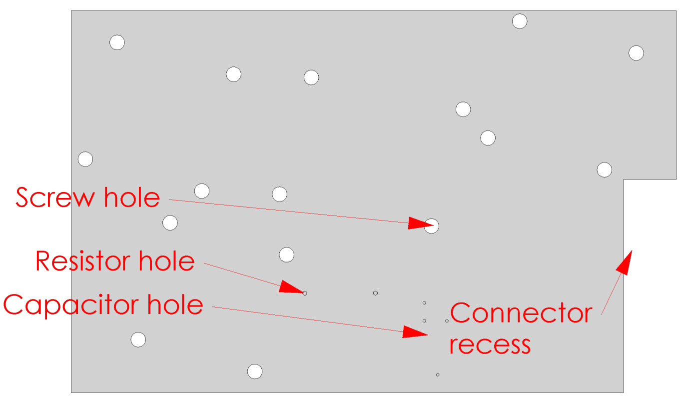


**Fig. 32** The FCB back plate, to seal the channels

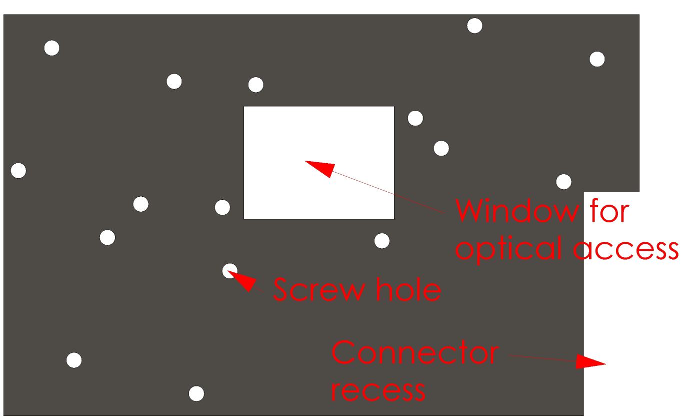


**Fig. 33** The FCB base plate, for easy assembly

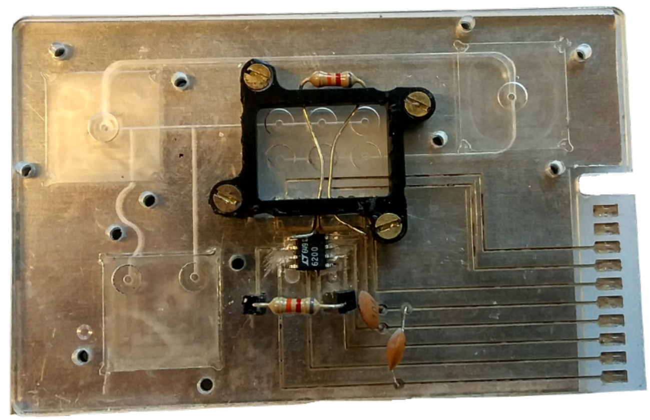

**Fig. 34** The assembled FCB

cause there are some problems, this is as easy as increasing the value of the electrode_spacing variable. For all the variables and a short description of these, see Table 3.

### SI.2.4 Modifications

For the next version of the FCB, the following modifications are recommended to make:

1. Exchange the IC for a through-hole variant, to ease the manufacturing. Right now, the IC is used as a surface-mounted device, but it is not enough to press it in the paste while manufacturing to affix it. Therefore, currently the IC is fixed using a droplet of Hysol glue and connected to the electrodes using Conductive Paint, leading to a more complex production process. A through-hole IC will be fixed when it is pressed in the paste when manufacturing, simplifying manufacturing;

2. If no longer needed, remove the electrode from the negative input of the IC towards the connector to reduce noise;

3. In order for the available flow sensor to be able to measure something, the bypass should be removed and one of the measurement channels should be attached to the output channel of the fertility chip, to maximize the pressure difference it will measure.

**Table 3** Variables used in the SOLIDWORKS model

| Variable | Description | Current value [mm] |
| --- | --- | --- |
| electrode_width | Width of the channels to be used as electrodes | 0.4 |
| electrode_spacing | Spacing between the channels to be used as electrodes | 1 |
| electrode_depth | Depth of the channels to be used as electrodes | 0.4 |
| capacitor_hole_size | Diameter of the capacitor holes | 0.4 |
| ic_depth | Depth of the pads for the IC | 0.6 |
| channel_depth | Depth of the microfluidic channels | 0.2 |
| channel_width | Width of the microfluidic channels | 0.2 |
| channel_corner_radius | Diameter of the microfluidic channel corners | 3.1 |
| recess_depth | Depth of the MFBB recesses | 0.4 |
| alignment_diameter | Diameter of the alignment holes for the resistors and capacitors | 1.6 |
| transition_distance | Distance to be used as transition from surface to recess electrode | 1 |
| fcb_height | Height of the substrate | 2 |
| bypass_diameter | Width of the microfluidic bypass | 0.8 |

## SI.3 PCB Design

To convert the output of the FCB electronics as explained in SI.2, a PCB has been developed which will also provide the FCB electronics with an input signal and the needed power supplies. It implements the part of the electronics as described in SI.1 which is not placed on the FCB, power conversion and additional amplification. It is also possible to choose the channel of the chip which should be used for the measurement. The design of the top layer of the PCB is depicted in Figure 35 and the design of the bottom layer in Figure 36. The full Bill of Materials (BOM) can be found in Table 5, including Farnell order code (can be used with the URL `http://nl.farnell.com/<order-code>`).

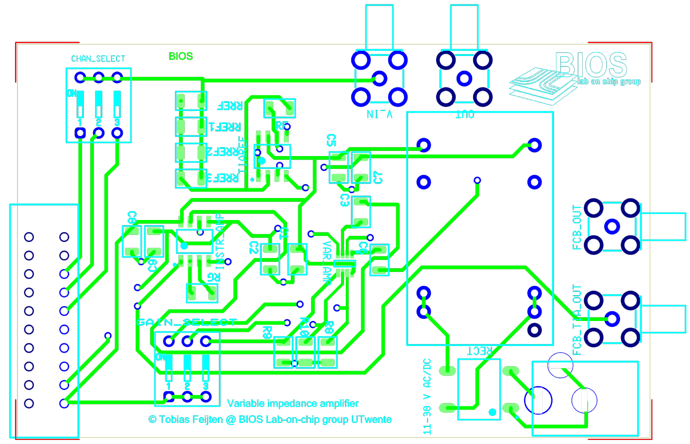


**Fig. 35** The top layer of the PCB

### SI.3.1 Power conversion

In order to power the circuit without the need for external symmetric power supplies, a DC-DC converter is present on the PCB which can be powered by 18-75 V DC and generates 5 V, ground and −5 V. In order to maximize the flexibility, a full diode bridge is present as well, meaning that the PCB can also be powered by AC (same voltage range as for DC). However, as these diodes induce a voltage drop of 1.1 V per piece, the voltage range which can be used to power the circuit changes to 20-77 V (*NOTE: On the produced PCB, this is erroneously described as 11-38 V!*).

### SI.3.2 Gain

On the PCB, an additional gain amplifier is present. This is implemented using a variable gain amplifier (LTC6910) and some switches to select the gain. The switches can influence the gain in a digital way. The resulting gains can be found in Table 4.

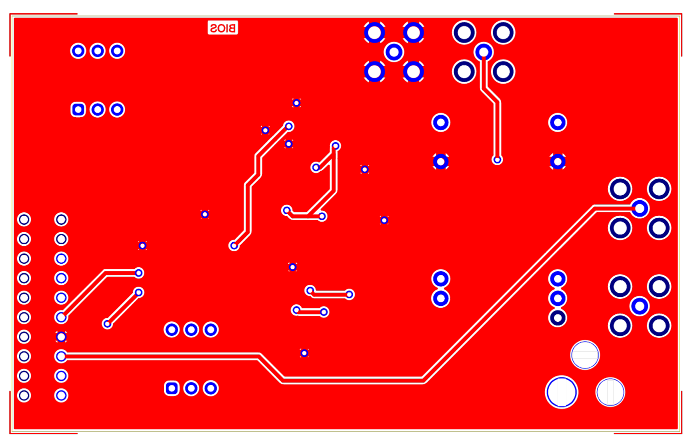

**Fig. 36** The bottom layer of the PCB

### SI.3.3 Modifications

The following modifications have been made to the original design in order to get the circuit working:

1. The ground and negative power supply rails of the FCB were switched around, which has been fixed (see Figure 40);

2. On the original design, the TIA was implemented using a Texas Instruments TLC271 op amp, which did not comply

**Table 4** Gain for different switch positions

| Switch 1 | Switch 2 | Switch 3 | Gain [V/V] |
|---|---|---|---|
| 0 | 0 | 0 | 0 |
| 0 | 0 | 1 | 1 |
| 0 | 1 | 0 | 2 |
| 0 | 1 | 1 | 5 |
| 1 | 0 | 0 | 10 |
| 1 | 0 | 1 | 20 |
| 1 | 1 | 0 | 50 |
| 1 | 1 | 1 | 100 |

with the bandwidth requirement. It has been switched with a LT6200 op amp, which requires pin 1 to be floating instead of connected to ground. Therefore, this pin is cut through;

3. In the simulations the instrumentation amplifier had the best performance with a very low gain resistor (very high gain). This led to offset due to noise to be amplified too much, so no usable signal could be obtained. The gain resistor was switched out for a 1.2 kΩ resistor, decreasing the gain of the instrumentation amplifier;

4. The output terminals are not connected to the ground, because this would damage the input of the lock-in amplifier. A wire is soldered to the ground plane to make diagnosis with an oscilloscope possible, see Figure 39. A better solution to make the ground accessible is to add a header pin connected to the ground plane.

For the next version of the PCB, the following modifications (alongside the ones mentioned previously, which were only done for 1 PCB) are recommended to be implemented:

1. Shorten the trace between pin 7 of the instrumentation amplifier and C3;

2. Either remove the FCB-out connector and associated trace, or shorten it as much as possible. This trace will introduce noise to the measured signal, as it acts like an antenna;

3. Use the lower voltage variant of the DC-DC converter (TEN 8-2421WI, Farnell order code 1772190, instead of TEN 8-4821WI), to lower the needed power supply voltage.

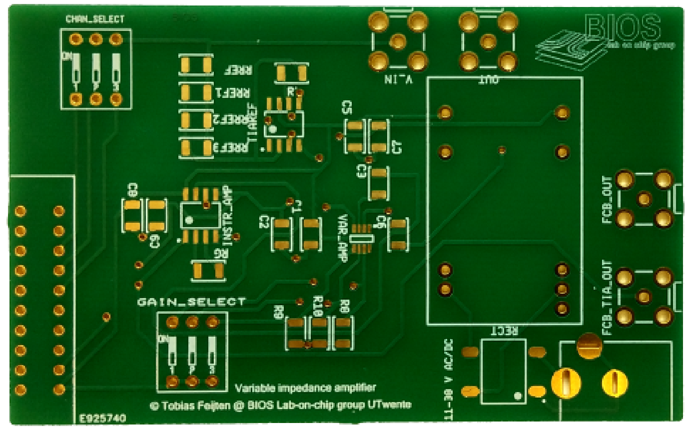


**Fig. 37** The top layer of the produced PCB

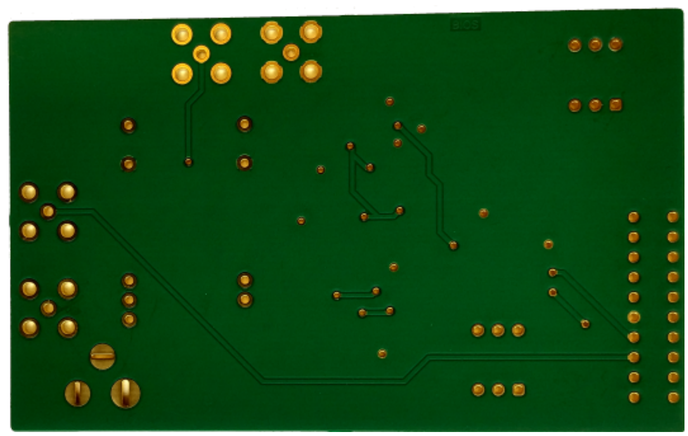

**Fig. 38** The bottom layer of the produced PCB

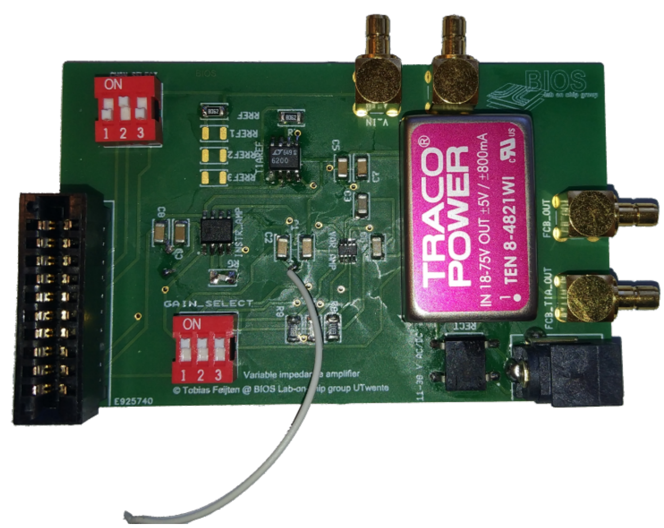


**Fig. 39** The top layer of the assembled PCB

**Table 5** Bill of materials for the PCB

| Quantity | Type of part | Value/part nr | Manufacturer | Farnell order code | On-board reference |
|---|---|---|---|---|---|
| 2 | Capacitor (DC decoupling) | $1\,\mu F$ | Multicomp | 1759454 | C3, C6 |
| 6 | Capacitor (power decoupling) | 100 nF | Multicomp | 1759366 | C1, C2, C5, C7, C8, C9 |
| 1 | Card edge connector (FCB) | 5-5530843-0 | TE Connectivity | 2396188 | Microfluidics |
| 1 | DC connector (power) | RAPC712X | Switchcraft | 1608726 | Power |
| 1 | DC-DC converter (generate symmetric power supply) | TEN8-4821WI | Tracopower | 1772198 | DCDC_conv |
| 2 | DIP-switch | MCNDS-03-V | Multicomp | 1255223 | CHAN_SELECT, Gain_select |
| 1 | Diode bridge (AC to DC) | DB102S | Multicomp | 1861404 | Rect |
| 1 | Instrumentation amplifier | AD8421ARZ | Analog Devices | 2126090 | Instr_amp |
| 1 | Variable gain amplifier | LTC6910-1CTS8 | Linear Technology | 1663930 | Var_amp |
| 1 | Operational amplifier (TIA) | LT6200CS8 | Linear Technology | 1330751 | TIAref |
| 3 | Resistor (pull-down) | $100\,k\Omega$ | Yageo | 9241060 | R8, R9, R10 |
| 1 | Resistor (instrumentation amplifier gain) | $10\,\Omega$ | Welwyn | 2078988 | Rg |
| 1 | Resistor (reference, should be similar to the FCB resistance) | $80\,k\Omega$ | Panasonic | 2307861 | Rref |
| 3 | Resistor (for tuning reference resistance) | optional | n.a. | n.a. | RREF1, RREF2, RREF3 |
| 1 | Resistor (feedback of reference TIA) | $80\,k\Omega$ | Panasonic | 2307861 | Rf |
| 4 | SMB connector | SMB1252B1-3GT30G-50 | Amphenol | 1111351 | FCB_out, FCB_TIA_out, Out, V_in |

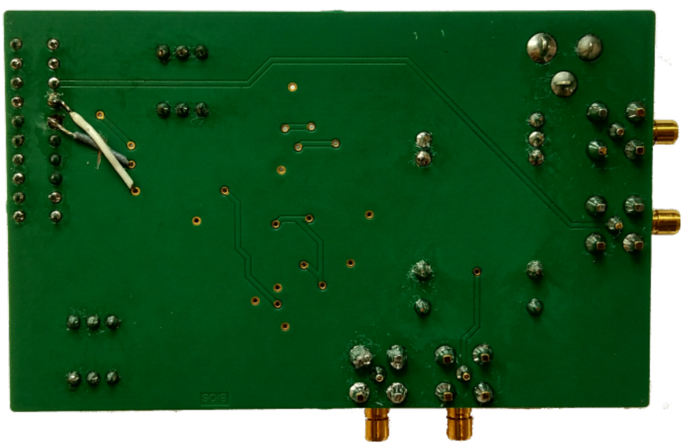

Fig. 40 The bottom layer of the assembled PCB

## SI.4 Clamp

In order to mount the chip on the FCB, a clamp has been designed based on the proposal from MFManufacturing[33]. The dimensions were adapted to fit the fertility chip, which has outer dimensions of 20 by 15 mm. The design can be found in Figure 41 (top) and Figure 42 (bottom). Some variables were defined in the SOLIDWORKS-model, in order to make changing the model very easy. The variables can be found in Table 6. The clamp has been manufactured using stereolithography, the result of which can be found in Figure 43 and Figure 44.

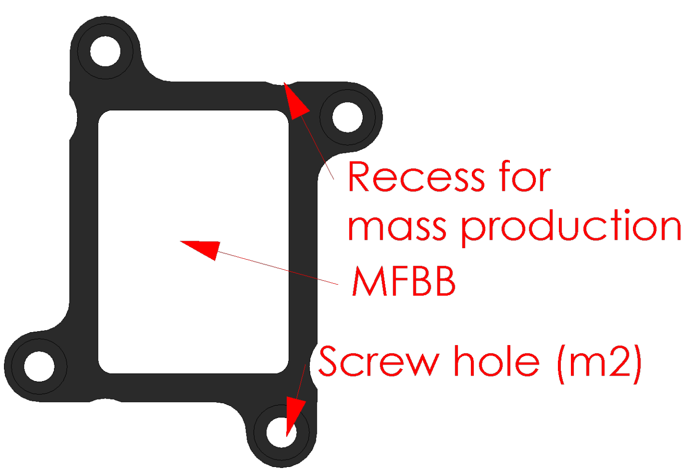


**Fig. 41** Top of the clamp design

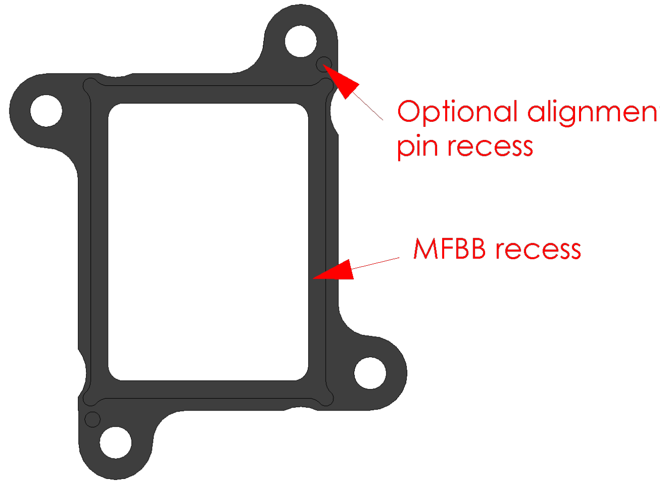


**Fig. 42** Bottom of the clamp design

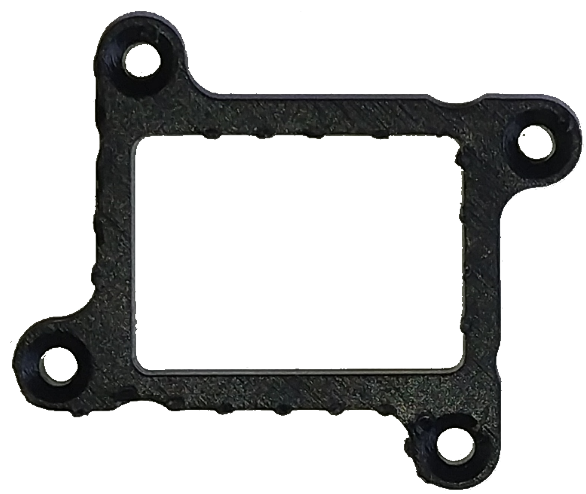

**Fig. 43** Top of the manufactured clamp

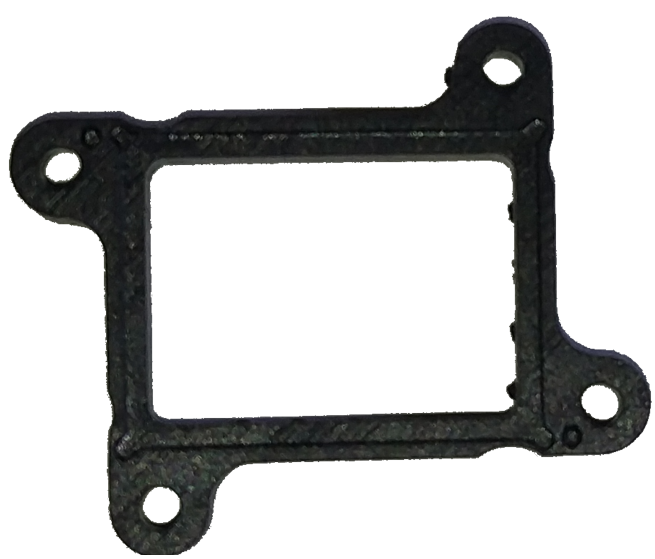

**Fig. 44** Bottom of the manufactured clamp

**Table 6** Variables used in the SOLIDWORKS model

| Variable | Description | Current value [mm] |
|---:|---:|---:|
| MFBB width | The width of the MFBB to be used with the clamp | 20.25 |
| MFBB length | The length of the MFBB to be used with the clamp | 15.25 |
| MFBB recess | The recess depth for the MFBB | 0.4 |
| Clamp thickness | The total thickness of the clamp | 4 |

## SI.5 Rapid prototyping

Microfluidic circuits can be fabricated using a couple of technologies, such as PDMS moulding, stereolithography (3D-printing), micromilling, glass processing, paperfluidics and hot embossing[34]. Of these technologies, stereolithography, micromilling, glass processing and hot embossing could be used to manufacture an FCB, as PDMS and paper lack the required rigidity for assembling MFBBs on them. A table with some of the characteristics of these methods compared can be found in Table 7.

Stereolithography is an additive fabrication method which uses a photoactivated polymer and a laser to selectively polymerize layers of a fluidic bath (sometimes also referred to as 3D-printing), which can be used to build up structures. It can also be used to create embedded channels, which creates the challenge of expelling the non-polymerized fluid from the channel. This makes the minimal channel diameter about $500\,\mu$m.

Micromilling is a subtractive fabrication method which uses mills and drills to selectively remove material from a bulk piece of material. This can be used with a broad range of materials, for instance polymers or metals. Using an automated milling machine, one can draw the desired structure in a CAD-program and use a CAM-program to produce the structure. The smallest structures depend on the mill size, which can get as small as $200\,\mu$m. Closed-off channels require the material to be bonded to another piece of material, which can create issues with alignment of structures.

Glass processing is also a subtractive fabrication method, but it entails a lot more than just creating structures. It can, for instance, also be used to create electrodes on the surface of the glass. Glass processing starts with a glass substrate, which can then be covered by photoresist which is selectively removed using photolithography. With the resist acting as a mask, glass can be removed using etching after which the resist is removed again. To create a channel, another glass substrate can be bonded to the existing structures. This production method is not really suited for large structures, as the etching and mask development for the photolithography take a long time. The channel size depends on the resist chemistry and lithography resolution. Sizes lower than $20\,\mu$m can be reached easily (the original fertility chip is made using this technology).

To perform hot embossing, one needs a mould with the desired structures as a negative. In this mould, a polymer is pressed while heated above the glass transition temperature of the polymer. This technology is particularly useful for making large amounts of structures, as the mould can be used multiple times. The mould can be created using stereolithography or micromilling. Since it is easier to create a very small ridge than create a very small valley, the feature size can shrink as well. To create channels, bonding is required again[34].

**Table 7** Comparison of fabrication methods

| **Method** | **Micromilling** | **3D-printing** | **Lithography + etching** | **3D-casting + hot embossing** |
|---|---|---|---|---|
| Cost | + | + | – (clean room) | +(+) (for high volumes) |
| Alignment | - (multiple layers) | ++ | ☐ (multiple layers) | - (multiple layers) |
| Channel size | ☐ (min. 200 $\mu$m) | - (min. 500 $\mu$m) | ++ (min. 20 $\mu$m) | + (min. 100 $\mu$m) |
| Speed | + | + | - | +(+) ( for high volumes) |
| Feature size | ☐ | - | ++ | ☐/+ |
| Material | COP/COC | Methacrylated polymer | Glass | COP/COC |
| Electrode integration | ☐ | ☐/- | + | ☐ |
| Biocompatibility | + | - | + | + |
| Chemical resistivity | + | - | ++ | + |

## SI.6 Description of electrode material differences

Two types of electrode materials were available, both in a paste form. One is based on carbon graphite (Gwent Electronic Materials, C2000802P2) and the other on silver/silver chloride (70/30) (Gwent Electronic Materials, C2051014P10). Their reported resistivities are, respectively $50\,\Omega/\mathrm{square}$ and $0.34\,\Omega/\mathrm{square}$. They are made to be applied on a substrate, then cured in an oven to set and attach. To determine the suitability for the application, an experiment was devised to compare the materials. A design was made for a 85x54mm COC substrate, using many lines of $65.5\,\mathrm{mm}$ length, with varying other dimensions, as depicted in Figure 45, which are then filled with the materials. After removing the superfluous material (using a windscreen wiper and, if necessary, some IsoPropanol Alcohol (IPA)) and curing in an oven at $60\,^{\circ}\mathrm{C}$ for multiple hours, the resistivity can be diagnosed using an Agilent 34401A multimeter set to resistance mode and two measurement probes, measuring at the far ends.

The finished substrates can be found in Figure 48 and Figure 49. When looking closely, some of the channels on the carbon graphite plate contain holes, caused by some of the paste being removed out of the channel by the windscreen wiper. The silver/silver chloride substrate doesn't seem to suffer from this problem. The resistance results can be found in Table 8, and have also been plotted in Figure 46 for carbon graphite and Figure 47 for silver/silver chloride. As can be seen, the resistance of the carbon graphite channels is much higher than the resistance of the silver/silver chloride channels. Furthermore, some of the carbon graphite channels have a much higher resistance than would be expected, which can be explained by the holes mentioned previously. Some detailed pictures have been made of both substrates as well, see Figure 50 and Figure 51.

Based on these results, we can say that for applications where a low resistivity of electrodes is required (which is helpful in most applications), the silver/silver chloride material will be the best choice. As for dimensions: for both materials, a larger channel leads to a lower resistance, meaning that a larger channel is more optimal for measurement purposes. As the resistance of

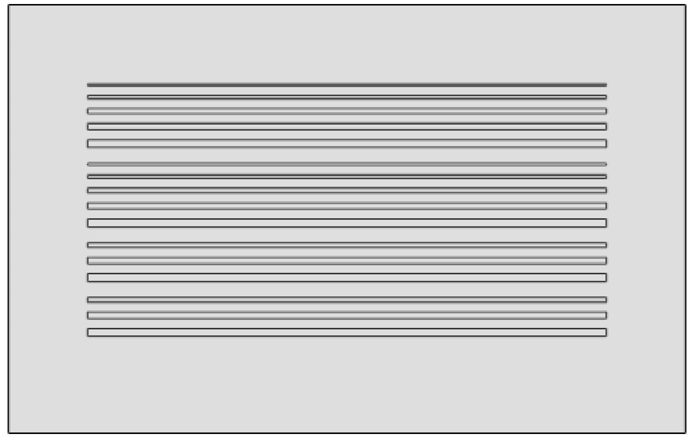

**Fig. 45** Design to test conductance of surface channels with electrode materials.

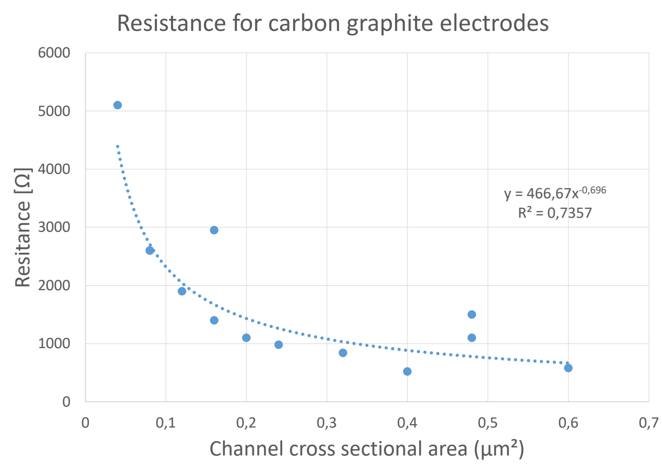


**Fig. 46** Resistance vs channel volume for carbon graphite electrodes

silver/silver chloride electrodes is much lower than the resistance we want to measure in this project, the dimensions are not that important. Because of space (which is limited on the FCB) and time (larger electrodes take a longer time to be milled), electrodes with a width of $400\,\mu\mathrm{m}$ and a depth of $400\,\mu\mathrm{m}$ will be used.

**Table 8** The resistance results for both materials

| Width [$\mu$m] | Height [$\mu$m] | Cross sectional area [$\mathrm{mm}^2$] | Resistance carbon graphite [$\Omega$] | Resistivity carbon graphite [$\Omega \cdot \mathrm{m}$] | Resistance silver/silver chloride [$\Omega$] | Resistivity silver/ silver chloride [$\Omega \cdot \mathrm{m}$] |
|---|---|---|---|---|---|---|
| 200 | 200 | 0,04 | 5100 | 3115 | 3,6 | 2,20 |
| 400 | 200 | 0,08 | 2600 | 3176 | 2,5 | 3,05 |
| 600 | 200 | 0,12 | 1900 | 3481 | 1,7 | 3,11 |
| 800 | 200 | 0,16 | 1400 | 3420 | 1,4 | 3,42 |
| 1000 | 200 | 0,2 | 1100 | 3359 | 1,3 | 3,97 |
| 200 | 400 | 0,08 | 2600 | 3176 | 2,6 | 3,18 |
| 400 | 400 | 0,16 | 2950 | 7206 | 1,4 | 3,42 |
| 600 | 400 | 0,24 | 980 | 3591 | 0,95 | 3,48 |
| 800 | 400 | 0,32 | 840 | 4104 | 0,71 | 3,47 |
| 1000 | 400 | 0,4 | 520 | 3176 | 0,58 | 3,54 |
| 600 | 600 | 0,36 | 11000 | 60458 | 0,74 | 4,07 |
| 800 | 600 | 0,48 | 1100 | 8061 | 0,52 | 3,81 |
| 1000 | 600 | 0,6 | 580 | 5313 | 0,39 | 3,57 |
| 600 | 800 | 0,48 | 1500 | 10992 | 0,58 | 4,25 |
| 800 | 800 | 0,64 | 96000 | 938015 | 0,42 | 4,10 |
| 1000 | 800 | 0,8 | 700 | 8550 | 0,39 | 4,76 |

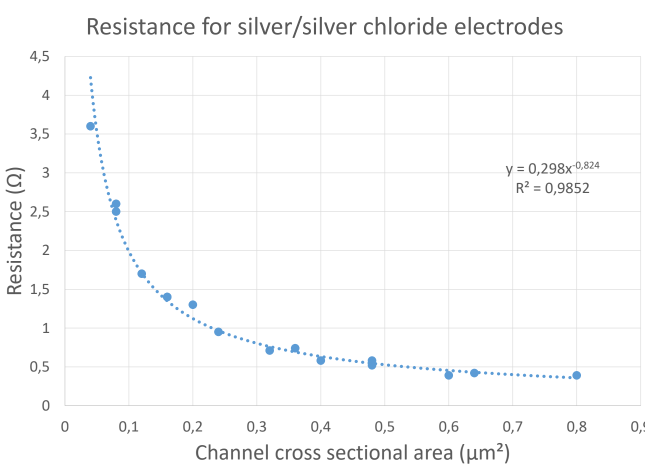


**Fig. 47** Resistance vs channel volume for silver/silver chloride electrodes

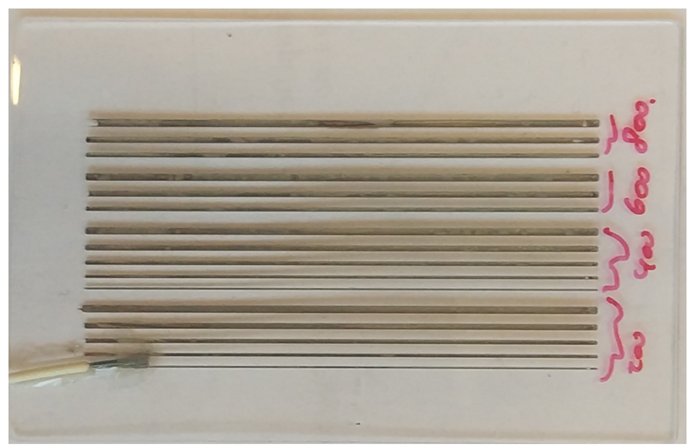

**Fig. 49** Overview of silver/silver chloride test substrate

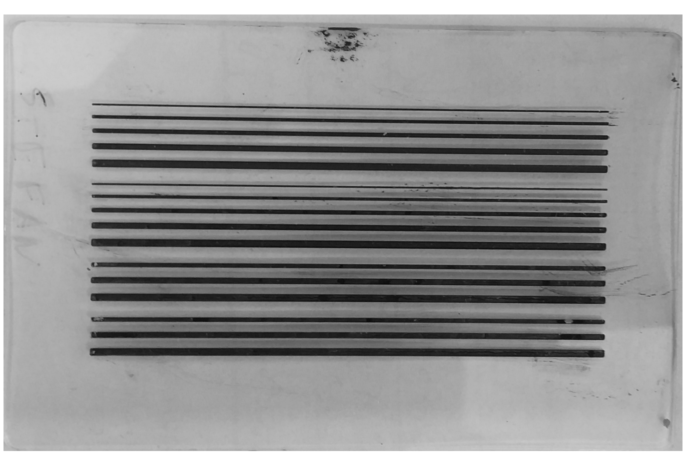

**Fig. 48** Overview of carbon graphite test substrate

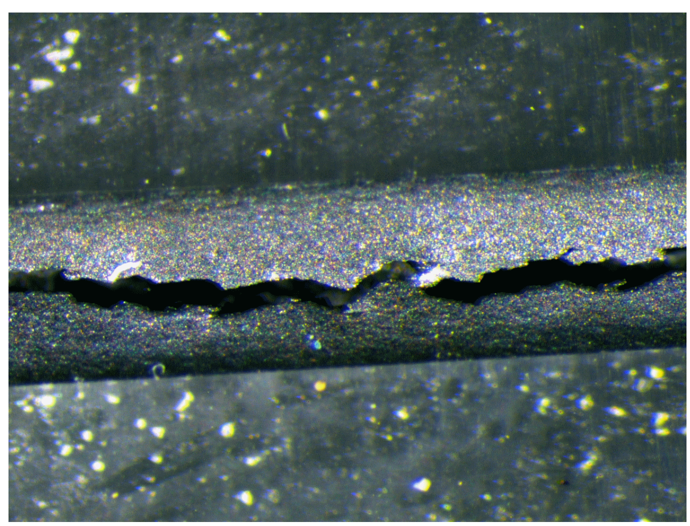

**Fig. 50** Detail shot of carbon graphite test substrate

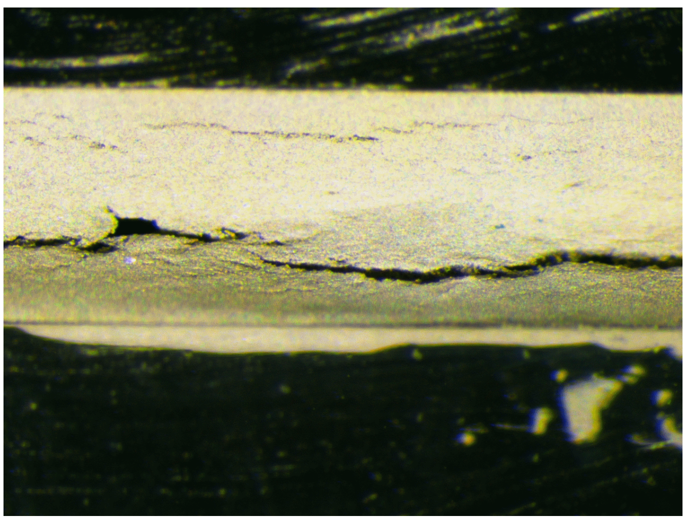

**Fig. 51** Detail shot of silver/silver chloride test substrate

## SI.7 Manufacture manual of FCB

| # | Front | Side | Description |
|---|---|---|---|
| 1 |  |  | Start with a 2 mm thick COC substrate. |
| 2 |  |  | Mill the rough parts of the recesses using a 2 mm mill. |
| 3 |  |  | Mill the electronics electrodes and the rest of the recesses using a 0.4 mm mill. |
| 4 |  |  | Drill the o-ring recesses using a 4 mm mill (to get a flat surface). |
| 5 | 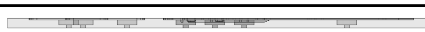 |  | Drill the fluidic in and outlets using a 1 mm drill. |
| 6 |  | 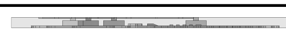 | Flip the substrate and mill the fluidic channels using a 0.2 mm mill. |
| 7 |  |  | Drill the bottom parts of the spring probe recesses using a 1 mm mill (to get a flat surface). |
| 8 |  | 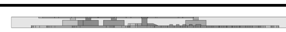 | Drill the spring probe holes using a 1.1 mm drill. |
| 9 | 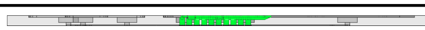 |  | Apply the conductive paste to the parts of the FCB around the spring probes, using a spatula and a windscreen wiper to remove excess paste. |
| 10 | 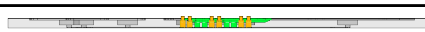 | 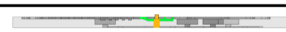 | Insert the spring probes in the holes (four outer and two middle ones), cure paste in oven for at least 2 hours @ 60 °C.<br>Test connectivity of probes with electrodes, if needed reapply paste and clean.<br>Fix any shorts between pogo pins by removing excessive ink, using a scalpel and, if needed, IsoPropyl Alcohol (IPA). |
| 11 | 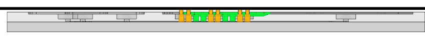 | 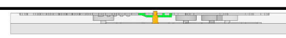 | Bond another 2 mm substrate to the channel side of the FCB:<br>1. Preheat the pneumatic press to 110 °C;<br>2. Expose the FCB and the new substrate to cyclohexane fumes for 4 minutes;<br>3. Press both FCB and the new substrate onto each other firmly, taking care that they're aligned;<br>4. Use the pneumatic press to press both substrates onto each other for 15 minutes. Use a pressure of 1500 kg;<br>5. Put small blocks of COC in the recesses, taking care the spring probes are not crushed by using a special block with a recess. Again, use the pneumatic press to improve the bond under the recesses. Use a pressure of 1500 kg and a temperature of 75 °C for 10 minutes;<br>6. Check the bond, if needed use additional pressure to improve it. |
| 12 | 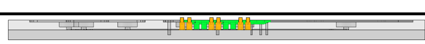 | 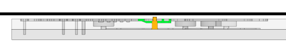 | Drill the resistor and capacitor holes from the top side using respectively a 0.6 mm and 0.4 mm drill. |
| 13 | 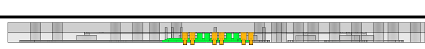 | 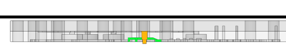 | Flip the FCB, drill the screw holes using a 2.1 mm drill. |
| 14 | 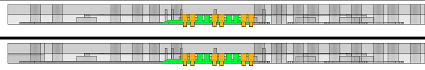 | 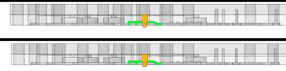 | Mill the recess for the card edge connector using a 2 mm mill. |

| | | | |
|---|---|---|---|
| 15 | 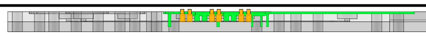 | 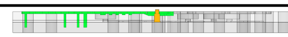 | Apply the conductive paste to the rest of the FCB, making sure a connection between the previously applied areas (in step 9) is achieved. |
| 16 | 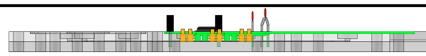 | 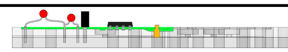 | Insert the headers for the resistor, the capacitors and the IC on the FCB.<br>Cure for at least 2 hours @ 60 °C. |